Chapter 6

P-i-N Rectifiers

It was demonstrated in the previous chapters that the on-state voltage drop of silicon Schottky barrier rectifiers becomes large when the device is designed to support more than 200 volts in the reverse blocking mode. Power device applications, such as motor control, require rectifiers with blocking voltages ranging from 300 volts to 5000 volts. Silicon P-i-N rectifiers have been developed for these high voltage applications. In a P-i-N rectifier, the reverse blocking voltage is supported across a depletion region formed with a P-N junction structure. The voltage is primarily supported within the n-type drift region with the properties of the p-type region optimized for good on-state current flow. Any given reverse blocking voltage can be supported across a thinner drift region by utilizing the punch-through design[1]. Since it is beneficial to use a low doping concentration for the n-type drift region in this design, it is referred to as an i-region (implying that the drift region is intrinsic in nature). The silicon P-i-N rectifiers that are designed to support large voltages rely upon the high level injection of minority carriers into the drift region. This phenomenon greatly reduces the resistance of the thick, very lightly doped drift region necessary to support high voltages in silicon. Consequently, the on-state current flow is not constrained by the low doping concentration in the drift region. A reduction of the thickness of the drift region, by utilizing the punch-through design, is beneficial for decreasing the on-state voltage drop.

In the case of silicon carbide rectifiers, the drift region doping level is relatively large and its thickness is much smaller than for silicon devices to achieve very high breakdown voltages. This enables the design of 4H-SiC based Schottky rectifiers with reverse blocking capability of upto at least 3000 volts with low on-state voltage drop. Based upon the inherent fast switching capability of Schottky rectifiers, it is anticipated that silicon carbide based Schottky rectifiers will displace silicon P-i-N rectifiers for applications with reverse blocking capability of upto

B.J. Baliga, *Advanced Power Rectifier Concepts*, DOI: 10.1007/978-0-387-75589-2_6,

© Springer Science + Business Media, LLC 2009

3000 volts[2]. However, this displacement will require further progress with reducing the cost of silicon carbide technology. Meanwhile, silicon P-i-N rectifiers will continue to play an important role in applications.

6.1 One-Dimensional Structure

The on-state current flow in the P-i-N rectifier is governed by three current transport mechanisms: (a) at very low current levels, the current transport is dominated by the recombination process within the space charge layer of the P-N junction – referred to as the *recombination current*; (b) at low current levels, the current transport is dominated by the diffusion of minority carriers injected into the drift region – referred to as the *diffusion current*; and (c) at high current levels, the current transport is dictated by the presence of a high concentration of both electrons and holes in the drift region – referred to as *high-level injection current*.

These current transport phenomena are discussed in detail in the textbook[1]. At the on-state operating current levels, current flow in the P-i-N rectifier is governed by the third process with injection of mobile carriers with concentrations far greater than the background doping concentration of the drift region. Only this process will be reviewed here for comparison with the physics of operation of the MPS rectifier that is discussed in the next chapter.

6.1.1 High Level Injection Current

The N-drift region in the P-i-N rectifier must be lightly doped in order to support high voltages in the reverse blocking mode. When the forward bias applied to the rectifier increases, the injected minority carrier concentration also increases in the drift region until it ultimately exceeds the background doping concentration (N_D) in the drift region. This is defined as *high level injection*. When the injected hole concentration in the drift region becomes much greater than the background doping concentration, charge neutrality requires that the concentrations for electrons and holes become equal:

$$n(x) = p(x) \qquad \textbf{[6.1]}$$

The large concentration of free carriers reduces the resistance of the drift region. This phenomenon is referred to as *conductivity modulation* of the drift region. Conductivity modulation of the drift region is beneficial for allowing the transport of a high current density through lightly doped drift regions with a low on-state voltage drop.

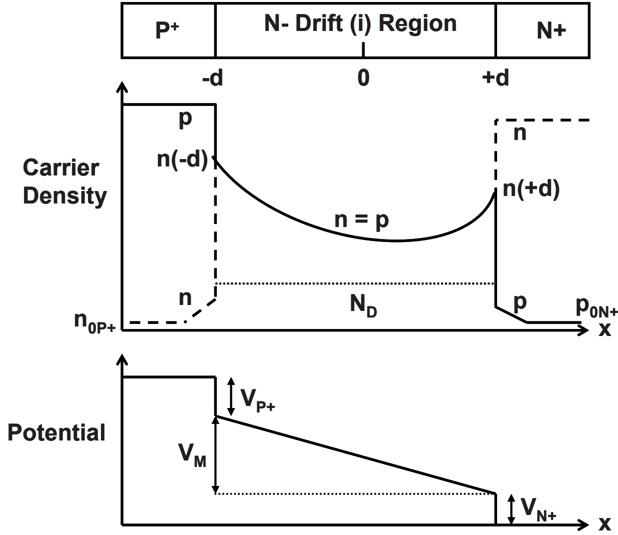

Fig. 6.1 Carrier and Potential Distribution under High-Level Injection Conditions for a P-i-N Rectifier.

The carrier distribution within the drift region n(x) can be obtained by solving the continuity equations for the N-region[3,4,5]:

$$\frac{\partial n}{\partial t} = -\frac{n}{\tau_{HL}} + D_n \frac{\partial^2 n}{\partial x^2} + \mu_n \frac{\partial}{\partial x}(nE) \qquad \textbf{[6.2]}$$

$$\frac{\partial p}{\partial t} = -\frac{p}{\tau_{HL}} + D_p \frac{\partial^2 p}{\partial x^2} - \mu_p \frac{\partial}{\partial x}(pE) \qquad \textbf{[6.3]}$$

where D_n and D_p are the diffusion coefficients for electrons and holes, respectively, and τ_{HL} is the high level lifetime in the drift region. Combining these equations after multiplying Eq. [6.2] by (μ_p.p) and Eq. [6.3] by (μ_n.n) gives:

$$\frac{\partial n}{\partial t} = -\frac{n}{\tau_{HL}} + \left(\frac{\mu_p p D_n + \mu_n n D_p}{\mu_p p + \mu_n n}\right)\frac{\partial^2 n}{\partial x^2} \qquad \textbf{[6.4]}$$

In deriving this equation, it has been assumed that the transport of carriers due to the electric field can be neglected when compared with the current due to the diffusion of the carriers. The Einstein relationship between the diffusion coefficient and the mobility gives:

$$D = \frac{kT}{q}\mu \qquad \textbf{[6.5]}$$

Since the carrier density for electrons and holes is equal in accordance with Eq. [6.1], Eq. [6.4] can be written under steady-state conditions as:

$$\frac{\partial n}{\partial t} = 0 = -\frac{n}{\tau_{HL}} + D_a \frac{\partial^2 n}{\partial x^2} \quad \textbf{[6.6]}$$

where D_a is the ambipolar diffusion coefficient given by:

$$D_a = \frac{p+n}{\dfrac{p}{D_n} + \dfrac{n}{D_p}} = \frac{2D_n D_p}{D_n + D_p} \quad \textbf{[6.7]}$$

due to charge neutrality (See Eq. [6.1]). The general solution for the carrier concentration governed by Eq. [6.6] is given by:

$$n(x) = A\cosh\left(\frac{x}{L_a}\right) + B\sinh\left(\frac{x}{L_a}\right) \quad \textbf{[6.8]}$$

with the constants A and B determined by the boundary conditions for the N-drift region. The parameter L_a in this equation, referred to as the *ambipolar diffusion length*, is given by:

$$L_a = \sqrt{D_a \tau_{HL}} \quad \textbf{[6.9]}$$

At the junction between the N-drift region and the N^+ cathode region (located at x = +d in Fig. 6.1), the total current flow occurs exclusively by electron transport:

$$J_T = J_n(+d) \quad \textbf{[6.10]}$$

and

$$J_p(+d) = 0 \quad \textbf{[6.11]}$$

Similarly, at the junction between the N-drift region and the P^+ anode region (located at x = –d in Fig. 6.1), the total current flow occurs exclusively by hole transport:

$$J_T = J_p(-d) \quad \textbf{[6.12]}$$

and

$$J_n(-d) = 0 \quad \textbf{[6.13]}$$

Using Eq. [6.11], the hole current due to drift and diffusion can be written as:

$$J_p(+d) = q\mu_p p(+d)E(+d) - qD_p\left(\frac{dp}{dx}\right)_{x=+d} = 0 \quad \textbf{[6.14]}$$

Combining this equation with Eq. [6.1] and the Einstein relationship:

$$E(+d) = \frac{kT}{qn(+d)}\left(\frac{dn}{dx}\right)_{x=+d} \quad \textbf{[6.15]}$$

Eq. [6.10] for the total current flow due to electron transport at this boundary can be written as:

$$J_T = q\mu_n n(+d)E(+d) + qD_n\left(\frac{dn}{dx}\right)_{x=+d} \quad \textbf{[6.16]}$$

Using Eq. [6.15] for the electric field E(+d):

$$J_T = 2qD_n\left(\frac{dn}{dx}\right)_{x=+d} \quad \textbf{[6.17]}$$

In the same manner:

$$J_T = 2qD_p\left(\frac{dn}{dx}\right)_{x=-d} \quad \textbf{[6.18]}$$

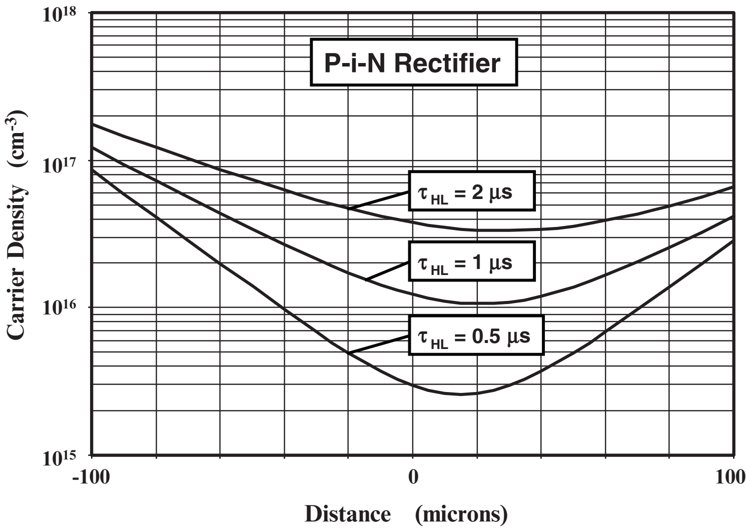

Fig. 6.2 Carrier Distribution under High-Level Injection Conditions for a P-i-N Rectifier with various High-Level Lifetime values.

The above boundary conditions can be used to obtain the constants A and B in Eq. [6.8] resulting in:

$$n(x) = p(x) = \frac{\tau_{HL} J_T}{2qL_a}\left[\frac{\cosh(x/L_a)}{\sinh(d/L_a)} - \frac{\sinh(x/L_a)}{2\cosh(d/L_a)}\right] \quad \textbf{[6.19]}$$

The catenary carrier distribution described by this equation was schematically illustrated in Fig. 6.1. As a particular example, the carrier distributions calculated by using Eq. [6.19] are shown in Fig. 6.2 for the case of three values for the high-level lifetime for a diode with drift region thickness of 200 microns. The largest concentrations for the electrons and holes in the drift region occur at its boundary with the P^+ and N^+ end-regions. The droop in the carrier density towards the center of the drift region is determined by the ambipolar diffusion length. A larger droop in concentration occurs with the smallest diffusion length, and a smaller average carrier concentration is observed when the lifetime is reduced.

The reduction of the average carrier density injected into the drift region with reduction of the lifetime can be deduced from charge control considerations. Under steady-state conditions, the current flow in the P-i-N rectifier can be related to sustaining the recombination of holes and electrons within the drift region if the recombination within the end-regions is neglected. Consequently:

$$J_T = \int_{-d}^{+d} qR\,dx \quad \textbf{[6.20]}$$

where R is the recombination rate given by:

$$R = \frac{n(x)}{\tau_{HL}} \quad \textbf{[6.21]}$$

Using an average carrier density (n_a) within the drift region, these equations can be combined to yield:

$$J_T = \frac{2qn_a d}{\tau_{HL}} \quad \textbf{[6.22]}$$

The average carrier density in the drift region is then given by:

$$n_a = \frac{J_T \tau_{HL}}{2qd} \quad \textbf{[6.23]}$$

From this relationship, it can be concluded that the average carrier density in the drift region will increase with the on-state current density and decrease with reduction of the lifetime. This behavior is exhibited by the carrier distribution in Fig. 6.2. For the case of an on-state current density of 100 A/cm^2 and a drift region thickness (2d) of 200 microns with a high-level lifetime of 1 microsecond, the

average carrier concentration obtained by using the above equation is 3 x 10^{16} cm^{-3}, which is consistent with the carrier distribution shown in Fig. 6.2.

The specific resistance of the drift region can be calculated from the average carrier density with the acknowledgement that both electrons and holes are available for current transport:

$$R_{i,SP} = \frac{2d}{q(\mu_n + \mu_p)n_a} \quad \textbf{[6.24]}$$

Using Eq. [6.23] for the average carrier density:

$$R_{i,SP} = \frac{4d^2}{(\mu_n + \mu_p)J_T \tau_{HL}} \quad \textbf{[6.25]}$$

The voltage drop across the drift region (middle-region) is then given by:

$$V_M = J_T.R_{i,SP} = \frac{4d^2}{(\mu_n + \mu_p)\tau_{HL}} \quad \textbf{[6.26]}$$

From this equation, it can be concluded that the voltage drop across the drift region is independent of the current density flowing through it. This unusual behavior occurs due to the presence of a high concentration of minority carriers, contrary to Ohm's law for drift regions without the conductivity modulation. Thus, the conductivity modulation phenomenon at high injection levels enables maintaining a low voltage drop across the drift region, which is extremely beneficial for obtaining a low on-state voltage drop in power P-i-N rectifiers.

A more accurate analysis of the voltage drop across the drift region can be performed by integration of the electric field. The electric field in the drift region can be obtained from the carrier distribution given by Eq. [6.19]. The hole and electron currents flowing in the drift region are given by:

$$J_p = q\mu_p \left(pE - \frac{kT}{q}\frac{dp}{dx} \right) \quad \textbf{[6.27]}$$

and

$$J_n = q\mu_n \left(nE + \frac{kT}{q}\frac{dn}{dx} \right) \quad \textbf{[6.28]}$$

The total current at any location in the drift region is constant and given by:

$$J_T = J_p + J_n \quad \textbf{[6.29]}$$

Combining these relationships:

$$E(x) = \frac{J_T}{q(\mu_n + \mu_p)n} - \frac{kT}{2qn}\frac{dn}{dx} \qquad \textbf{[6.30]}$$

Here, the charge neutrality condition n(x) = p(x) was also utilized. The first term in this expression takes into account the ohmic voltage drop due to current flow through the drift region. The second term in the expression is associated with the asymmetrical carrier gradient produced by the difference in the mobility for electrons and holes.

The integration of the electric field distribution given in Eq. [6.30] yields the voltage drop across the drift (or middle) region[5,6,7]

$$\frac{V_M}{kT/q} = \left\{ \begin{array}{l} \dfrac{8b}{(b+1)^2}\dfrac{\sinh(d/L_a)}{\sqrt{1-B^2\tanh^2(d/L_a)}} \\ .\arctan\left[\sqrt{1-B^2\tanh^2(d/L_a)}\sinh(d/L_a)\right] \end{array} \right\}$$

$$+ B\ln\left[\frac{1+B\tanh^2(d/L_a)}{1-B\tanh^2(d/L_a)}\right] \qquad \textbf{[6.31]}$$

where $b = (\mu_n/\mu_p)$ and $B = (\mu_n - \mu_p)/(\mu_n + \mu_p)$.

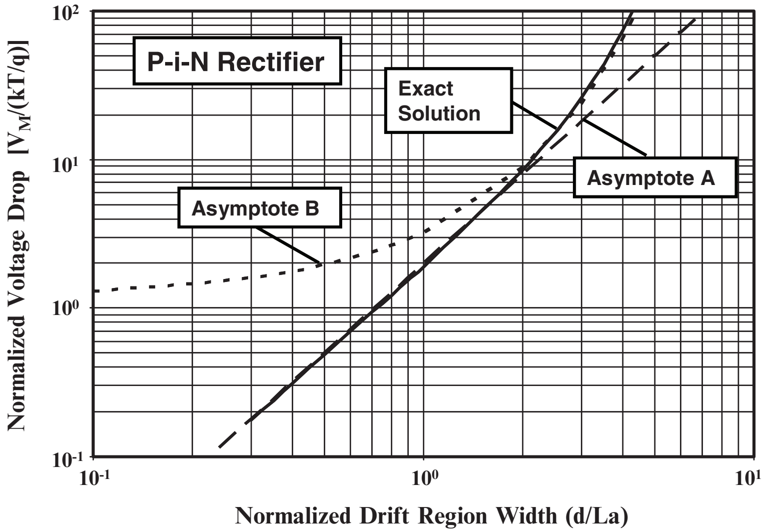

Fig. 6.3 Voltage Drop in the Drift (Middle) Region of a P-i-N Rectifier.

The above equation can be approximated by using two asymptotes as illustrated in Fig. 6.3. For d/L_a ratios of up to 2, the asymptote A given by:

$$V_M = \frac{2kT}{q}\left(\frac{d}{L_a}\right)^2 \quad \textbf{[6.32]}$$

provides a good fit. For d/L_a ratios of greater than 2, the asymptote B given by:

$$V_M = \frac{3\pi\, kT}{8q} e^{(d/L_a)} \quad \textbf{[6.33]}$$

provides a good fit. As discussed earlier in connection with Eq. [6.26], all these terms for the voltage drop across the drift region are independent of the on-state current density. The voltage drop across the drift region increases rapidly with increasing d/L_a ratio. When this ratio is 0.1, the middle region voltage drop is only 0.5 mV. It increases to a voltage drop of about 50 mV for a d/L_a ratio of unity and becomes 0.7 volts when the d/La ratio increases to 3. Thus, the increase in the voltage drop across the middle region degrades the on-state voltage drop when the lifetime is reduced in order to enhance the switching speed.

The on-state voltage drop in the P-i-N rectifier consists of the voltage drop across the P^+/N junction, the middle region, and the N/N^+ interface. The voltage drop across the P^+/N junction can be determined from the injected minority carrier density:

$$p(-d) = p_{0N} e^{\frac{qV_{P+}}{kT}} \quad \textbf{[6.34]}$$

where p_{0N} is the minority carrier density in the N-type drift region in equilibrium and V_{P+} is the voltage drop across the P^+/N junction. Relating the minority carrier concentration in equilibrium to the doping level N_D in the drift region:

$$V_{P+} = \frac{kT}{q}\ln\left[\frac{p(-d)N_D}{n_i^2}\right] \quad \textbf{[6.35]}$$

Similarly, applying the 'Law of the Junction' on the cathode side:

$$n(+d) = n_{0N} e^{\frac{qV_{N+}}{kT}} \quad \textbf{[6.36]}$$

where n_{0N} is the majority carrier density in the N-type drift region in equilibrium and V_{N+} is the voltage drop across the N^+/N junction. Since the majority carrier concentration in equilibrium is equal to the doping level N_D in the drift region:

$$V_{N+} = \frac{kT}{q}\ln\left[\frac{n(+d)}{N_D}\right] \quad \textbf{[6.37]}$$

The voltage drop associated with the two end regions is therefore given by:

$$V_{P+} + V_{N+} = \frac{kT}{q}\ln\left[\frac{n(+d)n(-d)}{n_i^2}\right] \quad \textbf{[6.38]}$$

In deriving this expression, the charge neutrality condition n(x) = p(x) under high level injection was assumed.

The voltage drop across the end regions has been combined with the voltage drop across the middle region to derive a relationship between the on-state current density (J_T) and the total on-state voltage drop (V_{ON}) for the P-i-N rectifier[3,4,5]

$$J_T = \frac{2qD_a n_i}{d} F\left(\frac{d}{L_a}\right) e^{\frac{qV_{ON}}{2kT}} \quad \textbf{[6.39]}$$

where

$$F\left(\frac{d}{L_a}\right) = \frac{(d/L_a)\tanh(d/L_a)}{\sqrt{1-0.25\tanh^4(d/L_a)}} e^{-\frac{qV_M}{2kT}} \quad \textbf{[6.40]}$$

From Eq. [6.39], it is apparent that, for a fixed on-state current density, the on-state voltage drop will be smaller if the function $F(d/L_a)$ is large.

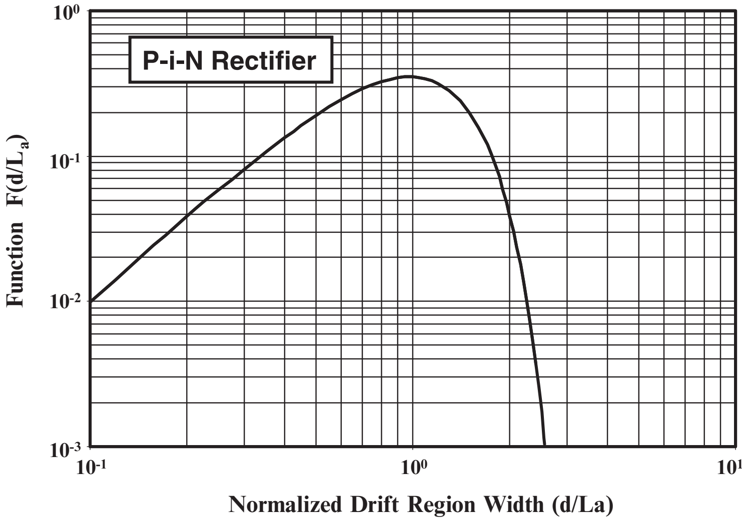

Fig. 6.4 Function $F(d/L_a)$ for a P-i-N Rectifier.

The variation of the function $F(d/L_a)$ with increasing (d/L_a) ratio is plotted in Fig. 6.4. It can be seen that this function has a maximum value when $d/L_a = 1$. Thus, in order to minimize the on-state voltage drop, the lifetime should be

adjusted until the diffusion length is equal to one-half of the width of the drift region. It is worth pointing out that the function $F(d/L_a)$ decrease very rapidly when the (d/L_a) ratio increases beyond a value of 3. This leads to a very rapid increase in the on-state voltage drop when the diffusion length is less than one-sixth of the drift region width.

The on-state voltage drop for a P-i-N rectifier can be derived from Eq. [6.39] for a device with its half-width (d) determined by the punch-through breakdown voltage capability:

$$V_{ON} = \frac{2kT}{q} \ln\left[\frac{J_T d}{2qD_a n_i F(d/L_a)}\right] \qquad \textbf{[6.41]}$$

The calculated on-state voltage drop for a silicon P-i-N rectifier with a drift region width of 200 microns is shown in Fig. 6.5 at an on-state current density of 100 A/cm^2. As expected, the on-state voltage drop exhibits a minimum at a (d/L_a) ratio of unity and increases rapidly when the (d/L_a) ratio exceeds 3.

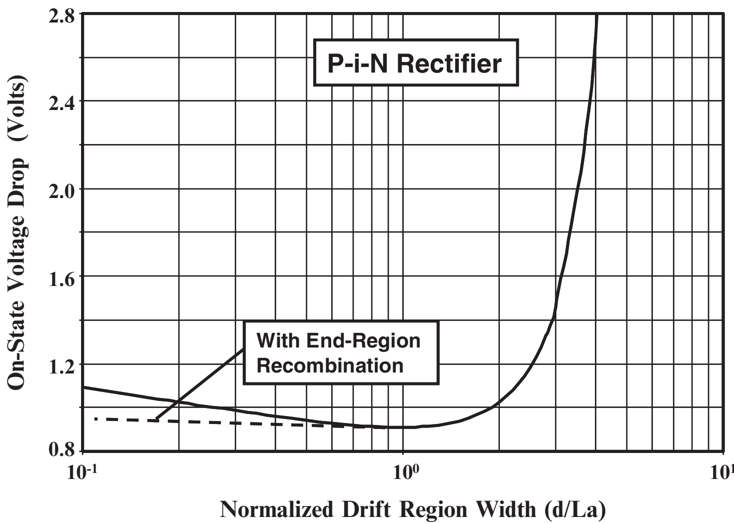

Fig. 6.5 On-state Voltage Drop for a P-i-N Rectifier.

6.1.2 Injection into the End-Regions

The high-level injection conditions within the drift region described above determine the on-state voltage drop at typical current densities in the range of 100 to 200 A/cm^2. At even greater on-state current densities, the injection of minority carriers into the end regions must be taken into account[6,7]. The total current flow must therefore accommodate not only the recombination of carriers in the drift region but also the recombination of carriers in the end regions. Thus:

$$J_T = J_{P+} + J_M + J_{N+} \quad \textbf{[6.42]}$$

Consequently, the current density associated with the middle region (J_M) is no longer equal to the total on-state current density (J_M) as assumed in the previous section but has a smaller value. This reduces the injection level in the drift region corresponding to any given total current density resulting in an increase in the voltage drop across the middle region.

Due to the high doping concentrations in the end regions, the injected minority carrier density in these regions is well below the majority carrier density even during operation at very high on-state current densities. The current corresponding to the end-regions can therefore be analyzed using low-level injection theory under the assumption of a uniform doping concentration in these regions. The current in the P+ region is given by[1]:

$$J_{P+} = \frac{qD_{nP+}n_{0P+}}{L_{nP+}\tanh\left(W_{P+}/L_{nP+}\right)}e^{\frac{qV_{P+}}{kT}} = J_{SP+}e^{\frac{qV_{P+}}{kT}} \quad \textbf{[6.43]}$$

where W_{P+} is the width of the P^+ region, L_{nP+} is the minority carrier diffusion length in the P^+ region, D_{nP+} is the minority carrier diffusion coefficient in the P^+ region, n_{0P+} is the minority carrier concentration in the P^+ region, and V_{P+} is the voltage drop at the P^+/N junction. In a similar manner:

$$J_{N+} = \frac{qD_{pN+}p_{0N+}}{L_{pN+}\tanh\left(W_{N+}/L_{pN+}\right)}e^{\frac{qV_{N+}}{kT}} = J_{SN+}e^{\frac{qV_{N+}}{kT}} \quad \textbf{[6.44]}$$

where W_{N+} is the width of the N^+ region, L_{pN+} is the minority carrier diffusion length in the N^+ region, D_{pN+} is the minority carrier diffusion coefficient in the N^+ region, p_{0N} is the minority carrier concentration in the N^+ region, and V_{N+} is the voltage drop at the N^+/N interface. In these equations, J_{SP+} and J_{SN+} are referred to as the *saturation current densities* for the heavily doped P^+ anode and N^+ cathode regions, respectively. They are a measure of the quality of the end regions as determined by their doping profiles and processing conditions. Typical values for the saturation current density are in the range from 1 x 10^{-13} to 4 x 10^{-13} amperes per cm^2 for silicon devices.

The injected carrier concentrations on the two sides of the P^+/N junction are related under quasi-equilibrium conditions by:

$$p_{P+}(-d).n_{P+}(-d) = p(-d).n(-d) \quad \textbf{[6.45]}$$

Under low-level injection conditions within the P^+ anode region:

$$p_{P+}(-d) = p_{0P+} \quad \textbf{[6.46]}$$

and

$$n_{P+}(-d) = n_{0P+}e^{\frac{qV_{P+}}{kT}} \quad \textbf{[6.47]}$$

Using these relationships in Eq. [6.45]:

$$p(-d).n(-d) = p_{0P+}.n_{0P+}e^{\frac{qV_{P+}}{kT}} = n_{ieP+}^2 e^{\frac{qV_{P+}}{kT}} \quad \textbf{[6.48]}$$

where n_{ieP+} is the effective intrinsic carrier concentration in the P^+ anode region including the influence of band-gap narrowing[1]. Due to charge neutrality considerations p(-d) = n(-d), leading to:

$$e^{\frac{qV_{P+}}{kT}} = \left[\frac{n(-d)}{n_{ieP+}}\right]^2 \quad \textbf{[6.49]}$$

Using this expression in Eq. [6.43]:

$$J_{P+} = J_{SP+}\left[\frac{n(-d)}{n_{ieP+}}\right]^2 \quad \textbf{[6.50]}$$

A similar derivation performed for the N^+ cathode side yields:

$$J_{N+} = J_{SN+}\left[\frac{n(+d)}{n_{ieN+}}\right]^2 \quad \textbf{[6.51]}$$

where n_{ieN+} is the effective intrinsic carrier concentration in the N^+ cathode region including the influence of band-gap narrowing. From these equations, it can be concluded that the carrier concentration in the drift region will increase as the square root of the current density if the end region recombination becomes dominant. Under these circumstances, the middle region voltage drop is no longer independent of the current density resulting in an increase in the total on-state voltage drop. The influence of end region recombination can be mitigated by optimization of the doping profile to minimize the saturation current densities.

6.1.3 Forward Conduction Characteristics

The analysis of current flow in a P-i-N rectifier in the previous sections indicates that the relationship between the current density and the voltage drop across the rectifier depends upon the injection level. At very low current levels, space charge generation controls the current flow with the current proportional to $(qV_{ON}/2kT)$. When the current is controlled by minority carrier injection into the drift region with the minority carrier concentration well below the background doping concentration, the current flow occurs by diffusion under low-level injection conditions. The current flow is then proportional to (qV_{ON}/kT). With further increase in the

forward current density, the injected carrier density in the drift region exceeds the background doping concentration leading to high level injection conditions. The current flow then once again becomes proportional to ($qV_{ON}/2kT$). In this mode of operation, the injected carrier concentration in the drift region increases in proportion to the current density resulting in a constant voltage drop across the drift region. At even larger on-state current densities, the influence of the recombination in the end-regions reduces the injected carrier density in the drift region. This produces a more rapid increase in the on-state voltage drop. This overall behavior is captured in Fig. 6.6 where a typical on-state characteristic is shown for a P-i-N rectifier under the various modes of operation.

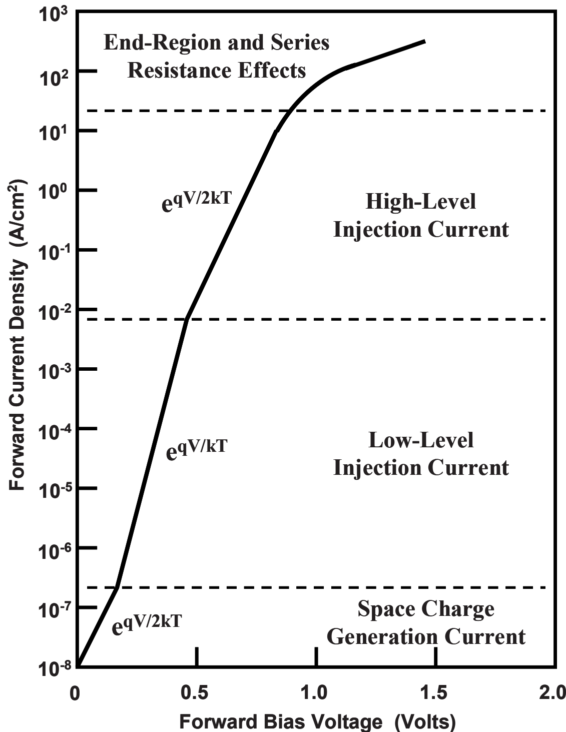

Fig. 6.6 On-state Characteristics for a P-i-N Rectifier.

Simulation Example

In order to gain further insight into the physics of operation for the P-i-N rectifier, the results of two-dimensional numerical simulations are provided in this section for a structure designed for supporting 3000 volts. For this case, a drift region with doping concentration of 4.6 x 10^{13} cm^{-3} was used with a thickness of 300 microns. The P^{+} and N^{+} end-regions had a surface concentration of 1 x 10^{19} cm^{-3} and a depth of about 5 microns. The on-state characteristics were obtained for various values for the lifetime (τ_{p0} and τ_{n0}). In all cases, it was assumed that $\tau_{p0} = \tau_{n0}$. The

influence of band-gap narrowing, auger recombination, and carrier-carrier scattering was included during the numerical simulations.

The on-state characteristics obtained from the numerical simulations are shown in Fig. 6.1E for the case of lifetime (τ_{p0} and τ_{n0}) of 10 microseconds in the drift region. Several distinct regimes of operation are apparent in the shape of the characteristics. At current densities ranging between 10^{-7} and 10^{-3} A/cm^2, the device operates in the low-level injection regime. Here, the slope of the i-v characteristic exhibits the expected (qV_{ON}/kT) behavior with the forward voltage drop increasing at the rate of 60 mV per decade of increase in the on-state current density. At larger current densities ranging between 10^{-3} and 10^{1} A/cm^2, the device operates in the high-level injection regime. Here, the slope of the i-v characteristic exhibits the expected ($qV_{ON}/2kT$) behavior with the forward voltage drop increasing at the rate of 120 mV per decade of increase in the on-state current density. This behavior validates the analytical theory described in the previous sections for current conduction in the P-i-N rectifier.

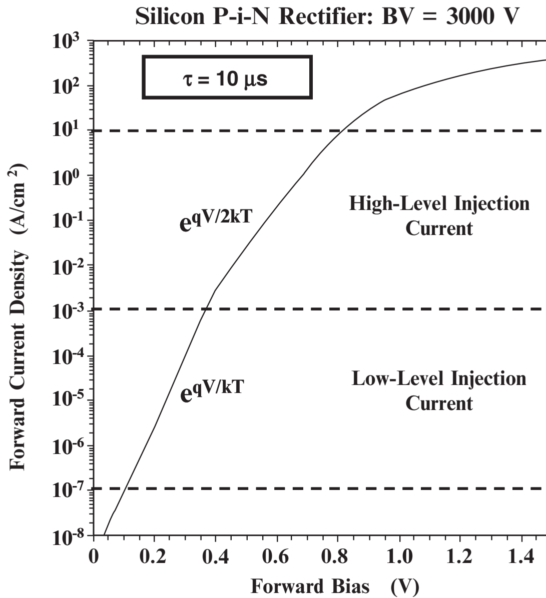

Fig. 6.1E On-state Characteristics for a 3000V Silicon P-i-N Rectifier.

The carrier distribution within the P-i-N rectifier is shown in Fig. 6.2E for the case of a lifetime (τ_{p0} and τ_{n0}) of 1 microsecond in the drift region at an on-state current density of 100 A/cm^2. Here, the hole concentration is shown with a solid line while the electron concentration is shown by a dashed line. It can be seen that high-level injection conditions prevail in the drift region because the injected carrier concentration is far greater than the background doping concentration. The hole and electron concentrations are equal in magnitude throughout the drift region and exhibit the expected catenary shape derived in the previous sections of this chapter. The average carrier concentration (4×10^{16} cm^{-3}) calculated by using Eq. [6.23] is in good agreement with the carrier density obtained from the simulations.

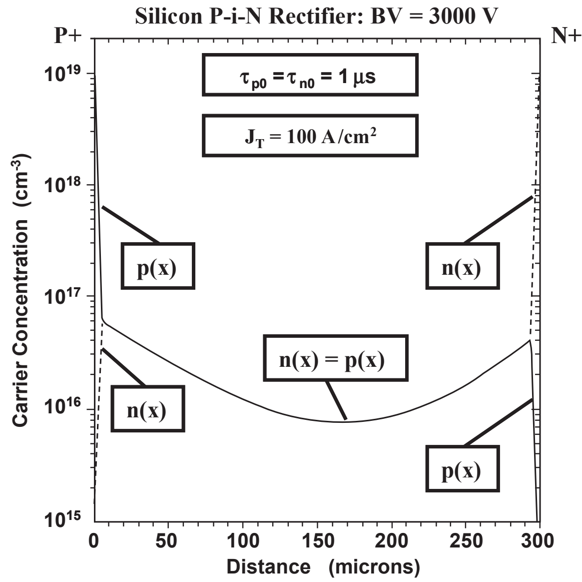

Fig. 6.2E Carrier Distribution within a 3000V P-i-N Rectifier.

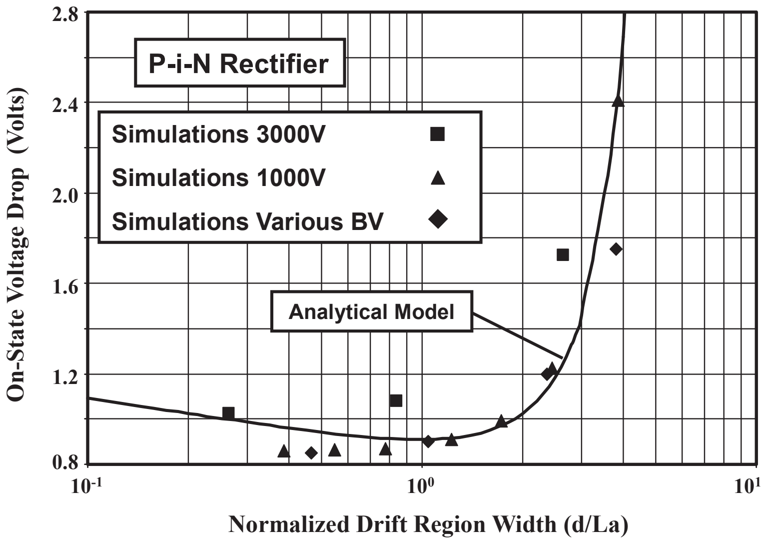

Fig. 6.3E On-State Voltage Drop for Silicon P-i-N Rectifiers.

The impact of changing the lifetime in the 3000V structure is shown in Fig. 6.3E. It can be seen that the on-state voltage drop is low for a lifetime of 100 microseconds. This is consistent with the small value of about 0.3 for the (d/L_a)

ratio. When the lifetime is reduced to 10 microseconds, the on-state voltage drop increases only slightly because the (d/L_a) ratio is still close to unity. However, the on-state voltage drop increases substantially when the lifetime is reduced to 1 microsecond because the (d/L_a) ratio has become significantly greater than one. The on-state voltage drop obtained with the simulations is close to that obtained using the analytical model, as shown in Fig. 6.3E by the square symbols, providing further credence to the model. In addition, the results obtained by varying the lifetime in a 1000 V P-i-N rectifier with an N-drift region width of 60 microns are shown by the triangular symbols.

During operation in power circuits, the junction temperature in the P-i-N rectifiers increases due to power dissipation. It is therefore important to evaluate the influence of the temperature upon the *i-v* characteristics in the forward conduction mode of operation. As an example, these characteristics are shown in Fig. 6.4E for the case of the 3000 V P-i-N rectifier with a lifetime (τ_{p0} and τ_{n0}) of 10 microseconds in the drift region. The on-state voltage drop at a forward current density of 100 A/cm^2 is observed to reduce slightly with temperature. This is due to a reduction of the voltage drop at the junctions. Unfortunately, this behavior favors the development of 'hot-spots' within devices where the current density can become large. However, the positive temperature coefficient for the on-state voltage drop for current densities above 300 A/cm^2 indicates stable operation is possible with only moderate non-uniformities in the current distribution within silicon P-i-N rectifiers.

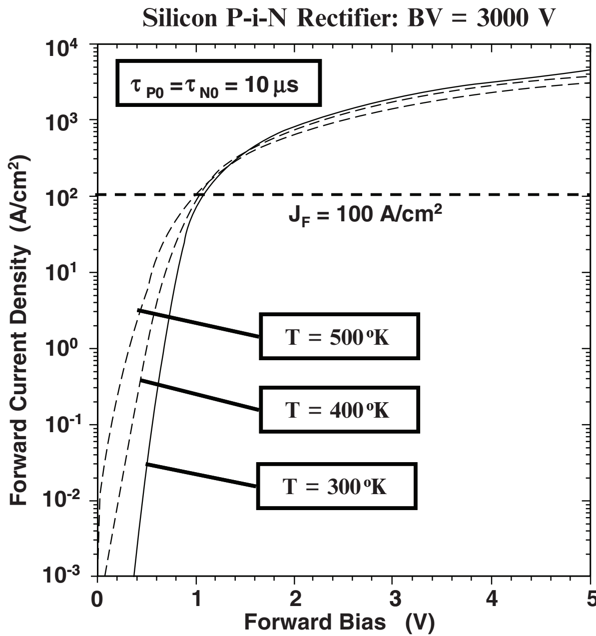

Fig. 6.4E Forward Conduction Characteristics of a Silicon P-i-N Rectifier.

6.2 Silicon Carbide P-i-N Rectifiers

Due to the much larger electric field that can be supported in silicon carbide, the width of the drift region is much smaller than that for the corresponding silicon device with the same breakdown voltage. This implies that the stored charge in the silicon carbide P-i-N rectifier will be much smaller than for the silicon device providing an improvement in the switching behavior. Unfortunately, the improved switching performance is accompanied by a substantial increase in the on-state voltage drop associated with the larger energy band gap for silicon carbide.

The physics of operation of the silicon carbide P-i-N rectifier is the same as that described in the previous sections. However, the parameters for the silicon carbide device defer from the silicon device. This has a strong impact on the voltage drop associated with the junctions. It was previous demonstrated that the junction voltage drop is given by:

$$V_{P+} + V_{N+} = \frac{kT}{q} \ln\left[\frac{n(+d)n(-d)}{n_i^2}\right] \quad \textbf{[6.52]}$$

Although the injected carrier concentrations n(+d) and n(-d) can be assumed to be similar in magnitude to those in a silicon P-i-N rectifier, the intrinsic carrier concentration for 4H-SiC is only 6.7 x 10^{-11} cm^{-3} at 300 ^{o}K, due to its larger energy band gap, when compared with 1.4 x 10^{10} cm^{-3} for silicon. This produces an increase in the junction voltage drop from 0.82 V for the silicon diode to 3.24 V for the 4H-SiC diode if the free carrier concentration in the drift region is assumed to be 1 x 10^{17} cm^{-3}. The power dissipation in the 4H-SiC P-i-N rectifier is therefore four times greater than in the silicon device. The expected improvement in the switching behavior is mitigated by the large on-state power loss. Consequently, it is preferable to develop silicon carbide Schottky diodes for voltage ratings of upto 5000 volts and P-i-N diodes for voltage ratings above 10,000 V.

Simulation Example

In order to illustrate the reduction in the stored charge within silicon carbide P-i-N rectifiers, consider the case of a 4H-SiC P-i-N rectifier designed to support 10,000 volts. The thickness of the drift region for this device is only 80 microns when compared with 1200 microns required for the silicon structure. The drift region also has relatively high doping level of 2 x 10^{15} cm^{-3}. Due to the smaller thickness, good conductivity modulation of the drift region is observed even for a very small lifetime (τ_{p0} and τ_{n0}) value of 100 ns as shown in Fig. 6.5E. However, poor conductivity modulation occurs for a typical lifetime (τ_{p0} and τ_{n0}) value of 10 ns in the drift region observed in 4H-SiC. Methods for improving the minority carrier lifetime in 4H-SiC are required to assure good diode characteristics. The plot in Fig. 6.5E was obtained at a forward bias of 4 volts because of the larger junction potential for 4H-SiC as discussed above. Thus, the improved switching performance is obtained at the significant disadvantage of high on-state power loss.

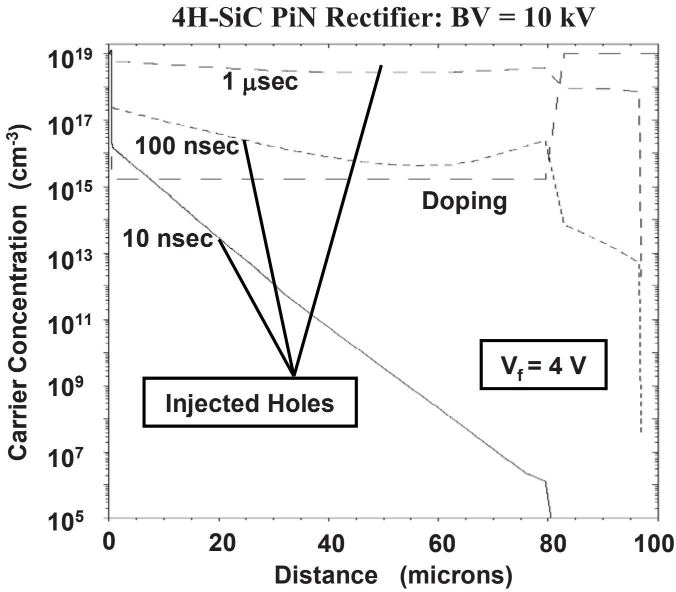

Fig. 6.5E Conductivity Modulation within 10 kV 4H-SiC PiN Rectifiers.

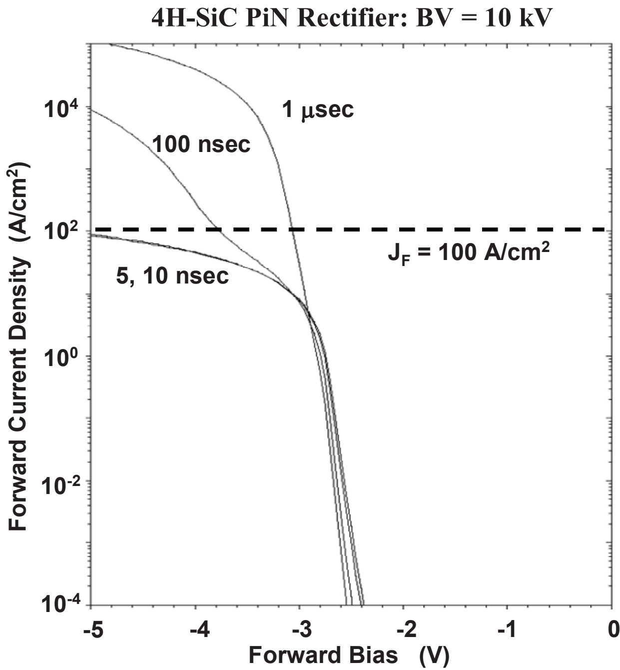

Fig. 6.6E Forward Conduction Characteristics of 10kV 4H-SiC PiN Rectifiers.

The forward i-v characteristics for the 10 kV 4H-SiC P-i-N rectifiers obtained from the numerical simulations are shown in Fig. 6.6E for various lifetime values. It can be observed that the on-state voltage drop is determined by the un-modulated resistance of the drift region when the lifetime is at 5 or 10 ns. When the lifetime is increased to 100 ns, the conductivity modulation of the drift region reduces the on-state voltage drop. With a lifetime of 1 microsecond, strong conductivity modulation occurs in the drift region as shown in Fig. 6.5E making the on-state voltage drop approximately 3 volts at an on-state current density of 100 A/cm^2. Lifetime values in this range have been more recently achieved and reported in silicon carbide devices[8].

6.3 Reverse Blocking

The reverse blocking voltage capability of the P-i-N rectifier is determined by the punch-through electric field distribution profile as described in the textbook[1]. The punch-through design enables reduction of the thickness of the drift region which is beneficial for reducing the on-state voltage drop as discussed in the previous sections of this chapter. Since the doping concentration of the drift region is small in the punch-through design, the drift region becomes completely depleted at a relatively low reverse bias voltage given by:

$$V_{PT} = \frac{qN_D(2d)^2}{2\varepsilon_S} \quad [6.53]$$

Beyond this voltage, the depletion region volume for the P-i-N rectifier remains independent of the reverse bias voltage under the assumption that the end-regions are heavily doped.

The leakage current for a reverse biased P-N junction is produced by a combination of the space charge generation current and the diffusion current. The space charge generation current, contributed by the carriers generated in the drift region, is given by:

$$J_{SC} = \frac{qW_D n_i}{\tau_{SC}} \quad [6.54]$$

where W_D is the width of the depletion region. An additional component of the leakage current is associated with the generation of electron-hole pairs in the neutral regions. Any minority carriers generated in the proximity of the junction diffuse to the depletion region boundary and get swept to the opposite side of the junction by the electric field. Under reverse blocking conditions, the diffusion components of the leakage current are given by:

$$J_{LN} = \frac{qD_p p_{0N}}{L_p} = \frac{qD_p n_i^2}{L_p N_D} \quad [6.55]$$

and

$$J_{LP} = \frac{qD_n n_{0P}}{L_n} = \frac{qD_n n_i^2}{L_n N_A} \qquad [6.56]$$

In the case of the P-i-N rectifier, the entire drift region is depleted at a relatively small reverse bias voltage due to its low doping concentration. The space charge generation current can therefore be assumed to arise from the entire width (2d) of the drift region while the diffusion currents are generated in the P^+ and N^+ end regions. The total leakage current for the P-i-N rectifier is then given by:

$$J_{LT} = \frac{qD_n n_i^2}{L_n N_{AP+}} + \frac{q(2d)n_i}{\tau_{SC}} + \frac{qD_p n_i^2}{L_p N_{DN+}} \qquad [6.57]$$

The influence of heavy doping effects on the intrinsic carrier concentration and the diffusion lengths can enhance the leakage current arising from the end regions. However, the leakage current in the P-i-N rectifier, under reverse blocking conditions, is determined primarily by the space-charge generation current. The contributions due to the diffusion currents from the end regions become comparable to the space-charge-generation current only at elevated temperatures.

As an example, consider the case of a P-i-N rectifier with a drift region with width (2d) of 100 microns and a space-charge-generation lifetime of 10 microseconds. The leakage current components calculated using Eq. [6.57] are plotted in Fig. 6.7 between 300 and 500 ^oK under the assumption that the P^+ and N^+ end-regions have a doping concentration of 1 x 10^{19} cm^{-3} and minority carrier

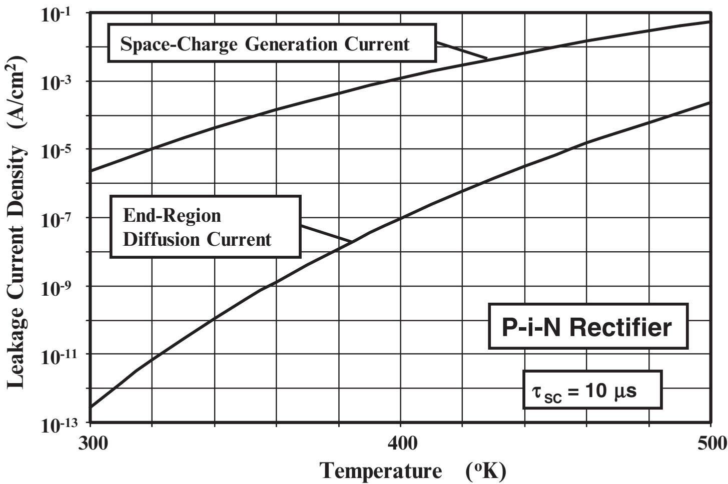

Fig. 6.7 Leakage Current Components in a Silicon P-i-N Rectifier.

lifetime of 1 ns. It is obvious that the leakage current due to the space-charge-generation process is dominant over this temperature range. It will therefore determine the total leakage current density in the silicon P-i-N rectifier.

Simulation Example

In order to validate the above model for the leakage current in the P-i-N rectifier, the results of numerical simulations on the 3000 V silicon P-i-N rectifier structure, whose forward characteristics were discussed a previous section, are described here. A reverse bias of 1000 volts was chosen to completely deplete the drift region. The leakage current was extracted over a temperature range of 300 to 500 ^{o}K. A lifetime (τ_{p0} and τ_{n0}) value of 10 microseconds was used in the drift region. The end regions had a Gaussian doping profile with a surface concentration of 1 x 10^{19} cm^{-3} and depth of about 10 microns. A leakage current density obtained using the simulations is compared with that calculated using the model in Fig. 6.7E. The excellent agreement between the calculated values and those obtained with the numerical simulations provides confirmation that the analytical model can be utilized for the analysis of the leakage current in P-i-N rectifiers.

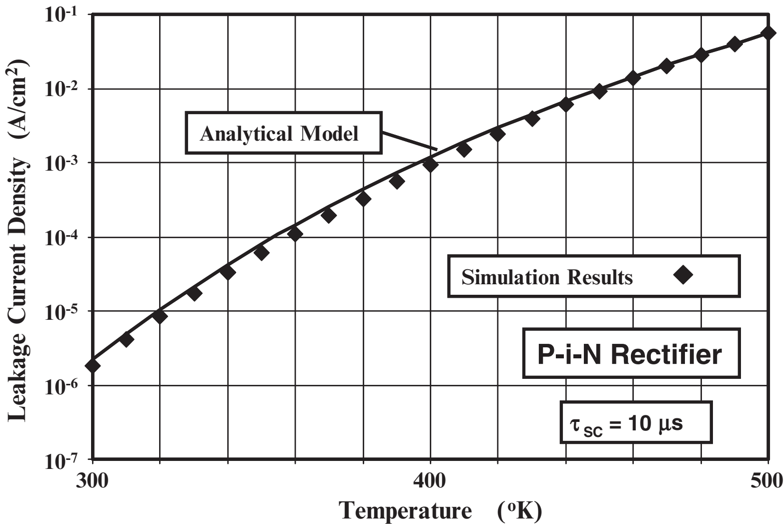

Fig. 6.7E Leakage Current in a 3kV Silicon P-i-N Rectifier.

6.4 Switching Performance

Power rectifiers control the direction of current flow in circuits used in various power conditioning applications. They operate for part of the time in the on-state when the bias applied to the anode is positive and for the rest of the time in the blocking state when the bias applied to the anode is negative. During each operating

cycle, the diode must be rapidly switched between these states to minimize power losses. Much greater power losses are incurred when the diode switches from the on-state to the reverse blocking state than when it is turned on. The stored charge within the drift region of the power rectifier produced by the on-state current flow must be removed before it is able to support high voltages. This produces a large reverse current for a short time duration. This phenomenon is referred to as *reverse recovery*.

The presence of a large concentration of free carriers in the drift region during on-state current flow is responsible for the low on-state voltage drop of high voltage silicon P-i-N rectifiers. In order to switch the diode from its on-state mode to the reverse blocking mode, it is necessary to remove these free carriers to enable the formation of a depletion region that can support a high electric field. The process of switching the P-i-N rectifier from the on-state to the blocking state is referred to as *reverse recovery*.

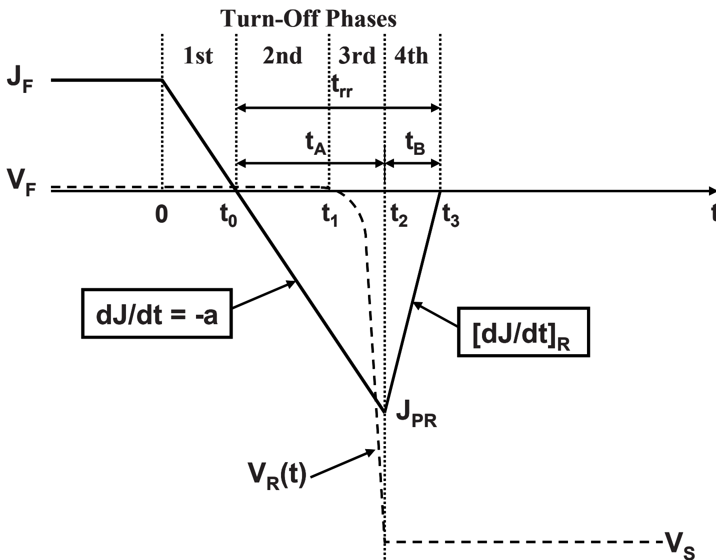

Fig. 6.8 Anode Current and Voltage Waveforms for the P-i-N Rectifier during the Reverse Recovery Process.

In power electronic circuits, it is common-place to use power rectifiers with an *inductive load*. In this case, the current reduces at a constant ramp rate (‘a’) as illustrated in Fig. 6.8 until the diode is able to support voltage. Consequently, a large *peak reverse recovery current* (J_{PR}) occurs due to the stored charge followed by the reduction of the current to zero. The power rectifier remains in its forward biased mode with a low on-state voltage drop until time t_1. The voltage across the diode then rapidly increases to the supply voltage with the rectifier operating in its reverse bias mode. The current flowing through the rectifier in the reverse direction reaches a maximum value (J_{PR}) at time t_2 when the reverse voltage becomes equal to the reverse bias supply voltage (V_S).

The simultaneous presence of a high current and voltage produces large instantaneous power dissipation in the power rectifier. The peak reverse recovery current also flows through the power switch that is controlling the switching event. This increases the power losses in the transistor. In the case of typical motor control PWM circuits that utilize IGBTs as power switches, a large reverse recovery current can trigger latch-up failure that can destroy both the transistor and the rectifier. It is therefore desirable to reduce the magnitude of the peak reverse recovery current and the time duration of the recovery transient. This time duration is referred to as the *reverse recovery time* (t_{rr}).

An analytical model for the reverse recovery process for the turn-off of a P-i-N rectifier under a constant rate of change of the current (*current ramp-rate*) can be created by assuming that the concentration of the free carriers in the drift region can be linearized as illustrated in Fig. 6.9[1]. As shown in the figure, the catenary carrier distribution established by the on-state current flow is approximated by an average value in the middle of the drift region and a linearly varying portion with a concentration of n(-d) at x = 0 to the average concentration of n_a at a distance x = b. These carrier concentrations can be obtained from Eq. [6.19] and Eq. [6.23]:

$$n(-d) = \frac{\tau_{HL} J_F}{2qL_a}\left[\frac{\cosh(-d/L_a)}{\sinh(d/L_a)} - \frac{\sinh(-d/L_a)}{2\cosh(d/L_a)}\right] \qquad \textbf{[6.58]}$$

and

$$n_a = \frac{J_F \tau_{HL}}{2qd} \qquad \textbf{[6.59]}$$

where J_F is the forward (or on-state) current density.

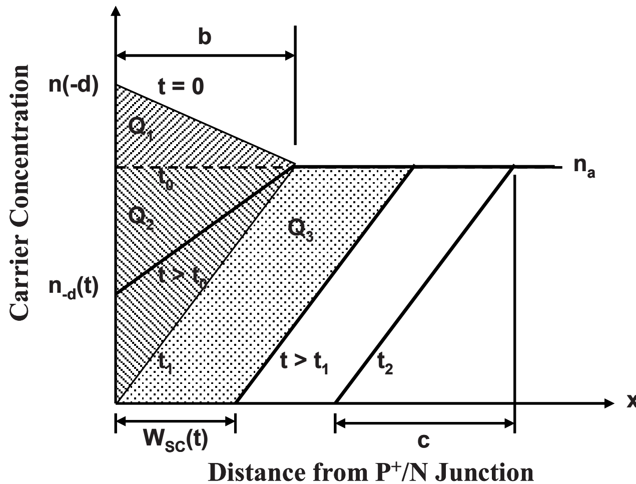

Fig. 6.9 Carrier Distribution Profiles in the P-i-N Rectifier during the Reverse Recovery Process.

The current flowing through the rectifier at any time during the turn-off transient is determined by the rate of diffusion of the carriers at the P^+/N junction boundary as described earlier during the discussion of on-state operation:

$$J_F = 2qD_a \left(\frac{dn}{dx} \right)_{x=-d} \quad \textbf{[6.60]}$$

In the first phase of the turn-off process, the current density in the P-i-N rectifier changes from the on-state current density (J_F) to zero at time t_0. The distance 'b' in Fig. 6.9 can be obtained by relating the charge Q_1 removed during the first phase to the current flow. At the end of the first phase, the carrier profile becomes flat at time t_0, as indicated by the dashed line in Fig. 6.9, because the current is zero at this time. The change in the stored charge within the drift region during the first phase can then be obtained from the cross-hatched area, indicated by Q_1, in the figure:

$$Q_1 = \frac{qb}{2}\left[n(-d) - n_a\right] \quad \textbf{[6.61]}$$

This charge can be related the current flow during the turn-off transient from $t = 0$ to $t = t_0$:

$$Q_1 = \int_0^{t_0} J(t)\,dt = \int_0^{t_0} (J_F - at)\,dt = J_F t_0 - \frac{at_0^2}{2} \quad \textbf{[6.62]}$$

The time t_0 at which the current crosses zero is given by:

$$t_0 = \frac{J_F}{a} \quad \textbf{[6.63]}$$

Combining the above relationships:

$$b = \frac{J_F^2}{qa\left[n(-d) - n_a\right]} \quad \textbf{[6.64]}$$

The carrier concentration n(-d) in Eq. [6.58] can be written as:

$$n(-d) = \frac{J_F \tau_{HL}}{2qL_a} K \quad \textbf{[6.65]}$$

where

$$K = \left[\frac{\cosh(-d/L_a)}{\sinh(d/L_a)} - \frac{\sinh(-d/L_a)}{2\cosh(d/L_a)} \right] \quad \textbf{[6.66]}$$

Using Eq. [6.65], in conjunction with Eq. [6.59], in Eq. [6.64]:

$$b = \frac{2dL_a J_F}{a\tau_{HL}\left(Kd - L_a\right)} \quad \textbf{[6.67]}$$

The distance ‘b’ can therefore be calculated from the device parameters (d and τ_{HL}), the on-state current density, and the ramp rate ‘a’.

The second phase of the turn-off process occurs from the time t_0 at which the current crosses zero upto the time t_1 when the P^+/N junction can begin to support voltage. The carrier profile at time t_1 is shown in Fig. 6.9 as extending from a zero concentration at the junction (located at x = 0) and the average concentration n_a at a distance ‘b’ from the junction. After time t_1, a depletion region forms at the P^+/N junction with the zero carrier concentration at some distance away from the junction. The time t_1 can be obtained by analysis of the charge removal during the turn-off transient from $t = t_0$ to $t = t_1$. In Fig. 6.9, the charge removed during this time interval is indicated by the cross-hatched area marked Q_2. This area is given by:

$$Q_2 = \frac{1}{2} q n_a b \quad \textbf{[6.68]}$$

This charge can be related the current flow during the turn-off transient from $t = t_0$ to $t = t_1$:

$$Q_2 = \int_{t_0}^{t_1} J\left(t\right) dt = \int_{t_0}^{t_1} \left(at\right) dt = \frac{a}{2}\left(t_1^2 - t_0^2\right) \quad \textbf{[6.69]}$$

Using Eq. [6.63] for t_0:

$$Q_2 = \frac{a}{2}\left(t_1^2 - \frac{J_F^2}{a^2}\right) \quad \textbf{[6.70]}$$

Combining Eq. [6.68] and Eq. [6.70]:

$$t_1 = \sqrt{\frac{q n_a b}{a} + \frac{J_F^2}{a^2}} \quad \textbf{[6.71]}$$

Making use of the Eq. [6.59] for the average carrier concentration n_a and Eq. [6.67] for the distance ‘b’:

$$t_1 = \frac{J_F}{a}\sqrt{\frac{L_a}{\left(Kd - L_a\right)} + 1} \quad \textbf{[6.72]}$$

Based upon this expression, the end of the second phase occurs earlier when the ramp rate is increased. This accelerates the point at which the rectifier can begin to support a reverse bias voltage.

During the entire time from t = 0 until time $t = t_1$, the P^+/N junction within the P-i-N rectifier remains forward biased because the minority carrier density in

the drift region at the junction [p(-d,t)] is above the equilibrium minority carrier concentration (p_{0N}). Under the assumptions of high level injection conditions in the drift region, the minority carrier density [p(-d,t)] is equal to the majority carrier density [n(-d,t)] that is illustrated in Fig. 6.9. Based upon Eq. [6.60], the current density at any point in time is given by:

$$J(t) = 2qD_a \left(\frac{dn}{dx} \right)_{x=-d} = 2qD_a \frac{[n(-d,t) - n_a]}{b} \quad \textbf{[6.73]}$$

The carrier concentration in the drift region at the junction is therefore related to the current density by:

$$p(-d,t) = n(-d,t) = n_a + \frac{J(t)b}{2qD_a} = n_a + \frac{(J_F - at)b}{2qD_a} \quad \textbf{[6.74]}$$

This expression is valid for both positive and negative values for the current density during the turn-off transient until time t_1. The voltage drop across the forward biased junction during this time interval can be obtained using the Boltzmann relationship:

$$V_F(t) = \frac{kT}{q} \ln\left[\frac{p(-d)}{p_{0N}} \right] = \frac{kT}{q} \ln\left[\frac{(J_F - at)b}{2qD_a p_{0N}} + \frac{n_a}{p_{0N}} \right] \quad \textbf{[6.75]}$$

This expression describes the change in the voltage drop across the P-i-N rectifier during the turn-off transient until it is able to support a reverse bias voltage.

During the third phase of the turn-off transient, the P-i-N rectifier begins to support an increasing voltage. This requires the formation of a space-charge region $W_{SC}(t)$ at the P^+/N junction that expands with time as illustrated in Fig. 6.9. The expansion of the space-charge region is achieved by further extraction of the stored charge in the drift region resulting in the reverse current continuing to increase after time t_1. The growth of the reverse bias voltage across the P-i-N rectifier can be analytically modeled under the assumption that the sweep out of the stored charge is occurring at an approximately constant current. In this case, the slope of the carrier distribution profile remains constant as shown in Fig. 6.9.

In Fig. 6.9, the charge removed at a time t, after the P^+/N junction is reverse biased at time t_1, is indicated by the shaded area marked Q_3. The area of this parallelogram is given by:

$$Q_3 = qn_a W_{SC}(t) \quad \textbf{[6.76]}$$

This charge can be related the current flow during the turn-off transient from time t_1 to time t:

$$Q_3 = \int_{t_1}^{t} J(t)\,dt = \int_{t_1}^{t} (J_F - at)\,dt = J_F(t - t_1) - \frac{a}{2}(t^2 - t_1^2) \quad \textbf{[6.77]}$$

Combining these relationships for the charge Q_3 provides an expression for the growth of the space-charge region as a function of time:

$$W_{SC}(t) = \frac{a}{2qn_a}\left(t^2 - t_1^2\right) - \frac{J_F}{qn_a}\left(t - t_1\right) \quad \textbf{[6.78]}$$

The voltage supported across this space-charge region can be obtained by solving Poisson's equation:

$$\frac{d^2V}{dx^2} = -\frac{dE}{dx} = -\frac{Q(x)}{\varepsilon_S} \quad \textbf{[6.79]}$$

where Q(x) is the charge in the space-charge region. Unlike the blocking mode of operation, where the charge in the depletion region consists of the ionized donor charge, during the turn-off process an additional charge is contributed by the large reverse current flow. This charge is due to the holes that are transiting through the space-charge region due to the removal of the stored charge. Since the electric field within the space-charge region is large, it can be assumed that these holes are moving at the saturated drift velocity ($v_{sat,p}$). The concentration of the holes within the space-charge region is then related to the current density (J_R) by:

$$p(t) = \frac{J_R(t)}{qv_{sat,p}} = \frac{(at - J_F)}{qv_{sat,p}} \quad \textbf{[6.80]}$$

The voltage supported by the space-charge region is then given by:

$$V_R(t) = \frac{q\left[N_D + p(t)\right]}{2\varepsilon_S} W_{SC}(t)^2 \quad \textbf{[6.81]}$$

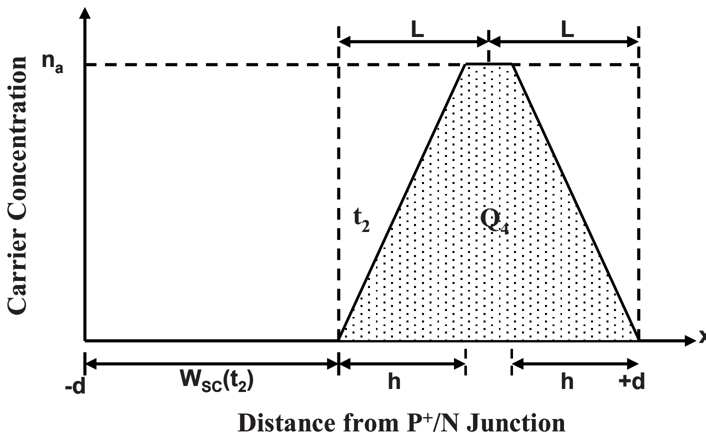

Fig. 6.10 Stored Charge within the P-i-N Rectifier after the end of the Third Phase.

This expression, in conjunction with Eq. [6.78] for the expansion of the space-charge width, indicates a rapid rise in the voltage supported by the P-i-N rectifier after time t_1. The end of the third phase occurs when the reverse bias across the P-i-N rectifier becomes equal to the supply voltage (V_S). Using this value in Eq. [6.81] together with Eq. [6.78], the time t_2 (and hence J_{PR}) can be obtained.

During the fourth phase of the turn-off process, the reverse current rapidly reduces at approximately a constant rate as illustrated in Fig. 6.8 while the voltage supported by the P-i-N rectifier remains constant at the supply voltage. The stored charge within the drift region after the end of the third phase is illustrated in Fig. 6.10 by the shaded area marked Q_4. At the end of the third phase of the turn-off process ($t = t_2$), the peak reverse recovery current J_{PR} is flowing through the structure. This current can be related to the free carrier profile by:

$$J_{PR} = 2qD_a \frac{dn}{dx} = 2qD_a \frac{n_a}{h} \quad \textbf{[6.82]}$$

where the dimension 'h' is shown in the Fig. 6.10. Using this equation:

$$h = \frac{2qD_a n_a}{J_{PR}} \quad \textbf{[6.83]}$$

The stored charge remaining in the drift region at time t_2 is then given by:

$$Q_4 = qn_a\left[2d - W_{SC}(t_2) - h\right] \quad \textbf{[6.84]}$$

This charge must be removed during the fourth phase of the turn-off process. During the fourth phase, the current reduces to zero at an approximately constant rate, indicated as $[dJ/dt]_R$ in Fig. 6.8, over a time period t_B extending from time t_2 to t_3. The charge removed due to the current flow during this time is given by:

$$Q_R = \frac{1}{2} J_{PR} t_B \quad \textbf{[6.85]}$$

This can be equated to the charge left in the drift region at the end of the third phase if recombination during this time is neglected due to the short duration of this time interval relative to the minority carrier lifetime. The time interval (t_B) for the reduction of the reverse current is then obtained:

$$t_B = (t_3 - t_2) = \frac{2qn_a}{J_{PR}}\left[2d - W_{SC}(t_2) - h\right] \quad \textbf{[6.86]}$$

The reverse ramp rate is then given by dividing the peak reverse recovery current by this time interval:

$$\left[\frac{dJ}{dt}\right]_R = \frac{J_{PR}}{t_B} = \frac{J_{PR}^2}{2qn_a\left[2d - W_{SC}\left(t_2\right) - h\right]} \qquad \textbf{[6.87]}$$

A smaller value for the reverse [di/dt] is desirable to reduce voltages developed across stray inductances in the circuit. These voltages cause an increase in the voltage supported by all the devices in the circuit making it necessary to enhance their breakdown voltages. This is detrimental to system performance due to an overall increase in power dissipation in the semiconductor components.

The utility of the analytical model can be illustrated by performing the analysis of the reverse recovery for a specific P-i-N rectifier structure. Consider the case of a P-i-N rectifier designed to support 1000 volts with a drift region thickness of 60 microns and doping concentration of 5 x 10^{13} cm^{-3}. The reverse recovery process in this structure is analyzed here using the analytical solutions for various ramp rates, lifetime values, and reverse supply voltages. In all cases, the reverse recovery is assumed to begin with on-state operation at a current density of 100 A/cm^2.

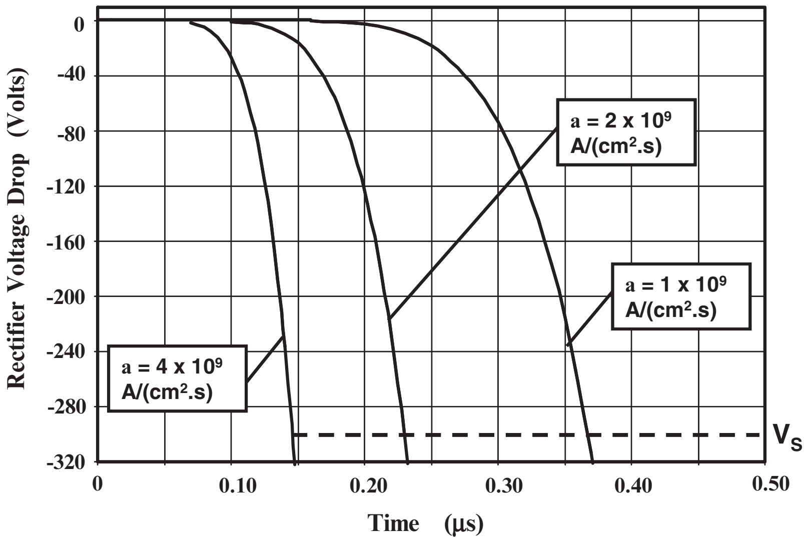

Fig. 6.11 Analytically Calculated Voltage Waveforms for a 1000 V P-i-N Rectifier during the Reverse Recovery Process using various Ramp Rates.

The voltage waveform calculated using the analytical solutions are shown in Fig. 6.11 for the case of a high level lifetime of 0.5 micro-seconds. With this lifetime, the average free carrier concentration in the drift region was found to be 5.2 x 10^{16} cm^{-3} for this structure at the on-state current density of 100 A/cm^2. According to the analytical model (see Eq. [6.71], the time t_1 at which the junction becomes reverse biased increases from 51 nanoseconds to 80 nanoseconds to 134 nanoseconds as the ramp rate decreases from 4 x 10^9 A/cm^2-s to 2 x 10^9 A/cm^2-s to

1×10^9 A/cm^2-s. Before this time, the voltage across the rectifier is slightly positive with a value given by Eq. [6.75]. The voltage then increases rapidly and reaches 300 volts (indicated by the dashed line in the figure) at 145, 230, and 370 nanoseconds, respectively, for the three cases. This point in the voltage waveforms defines the end of the third phase.

The peak reverse recovery current occurs at the end of the third phase. The peak reverse recovery current densities predicted by the analytical model are 480, 360, and 270 A/cm^2, respectively, for the three cases of the ramp rate as can be observed in Fig. 6.12 which shows the current waveforms obtained using the analytical model. After the third phase, the reverse current reduces to zero at a constant rate. The time duration (t_B), during which the reverse current reduces to zero, becomes smaller with a reduction in the ramp rate. The values for t_B predicted by the analytical model decrease from 70 to 60 to 28 nanoseconds as the ramp rate decreases from 4×10^9 A/cm^2-s to 2×10^9 A/cm^2-s to 1×10^9 A/cm^2-s. These combinations of the peak reverse recovery current and period t_B produce a reverse [dJ/dt] ranging from 6 to 9.5×10^9 A/cm^2-s.

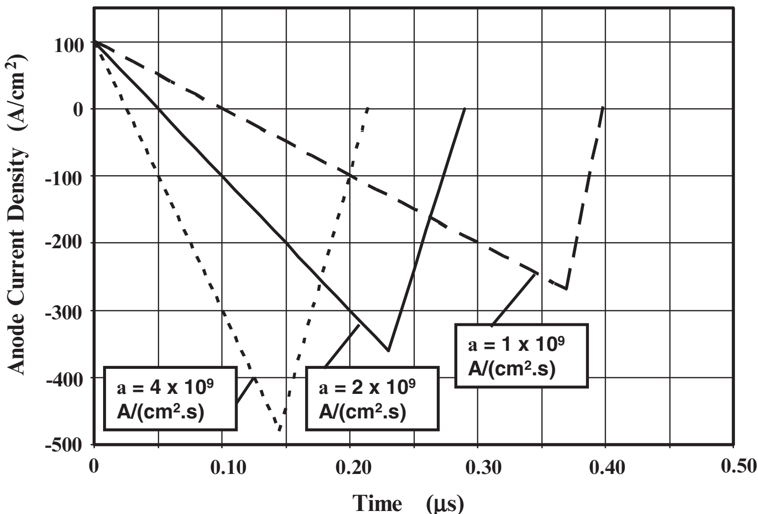

Fig. 6.12 Analytically Calculated Current Waveforms for a 1000 V P-i-N Rectifier during the Reverse Recovery Process using various Ramp Rates.

The analytical model can also be utilized to examine the influence of the minority carrier lifetime on the reverse recovery process. Consider the case of the same 1000-V P-i-N rectifier structure switched off from an on-state current density of 100 A/cm^2 at a ramp rate of 2×10^9 A/cm^{2}s. The voltage waveforms predicted by the analytical model for the reverse recovery process with lifetime values of 0.25, 0.5, and 1 microsecond in the drift region are shown in Fig. 6.13. The model predicts no change in the time t_1 for the end of the first phase and a faster rate of increase in the anode voltage during the second phase when the lifetime is reduced.

The current flow during the reverse recovery process is shown in Fig. 6.14 for the case of the three lifetime values. The peak reverse recovery current density predicted by the analytical model reduces from 480 to 360 to 270 A/cm^2, respectively, when the lifetime is reduced from 1 to 0.5 to 0.25 microseconds as

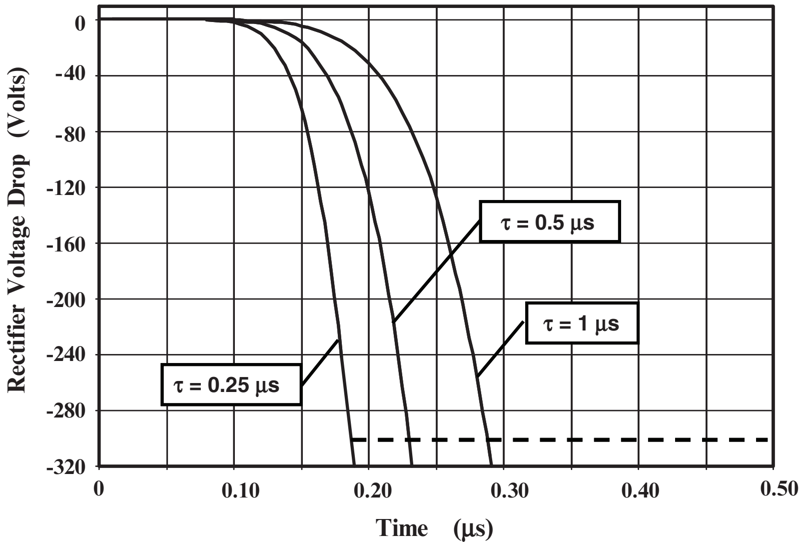

Fig. 6.13 Analytically Calculated Voltage Waveforms for a 1000 V P-i-N Rectifier during the Reverse Recovery Process for various Lifetime Values.

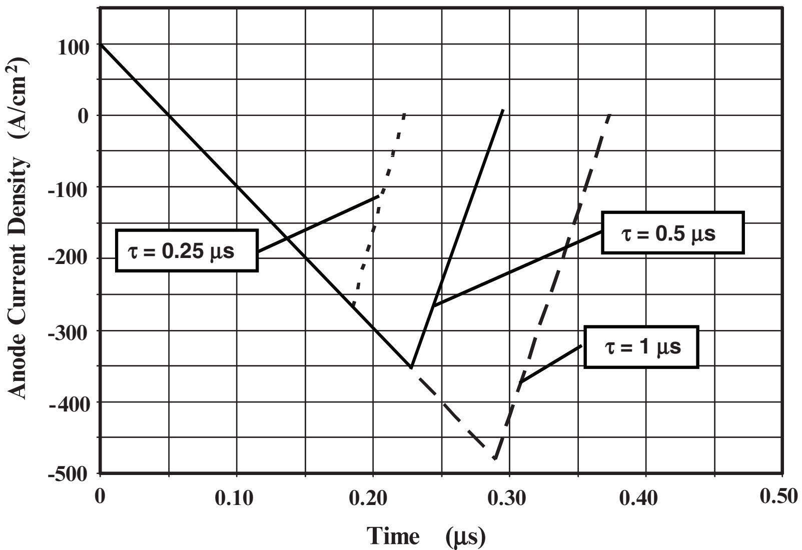

Fig. 6.14 Analytically Calculated Current Waveforms for a 1000 V P-i-N Rectifier during the Reverse Recovery Process for various Lifetime Values.

can be observed from Fig. 6.14. The time duration (t_B) for the fourth phase, during which the reverse current reduces to zero, also becomes smaller with a reduction in the lifetime. The values for t_B predicted by the analytical model are 38 nanoseconds, 60 nanoseconds, and 84 nanoseconds for lifetime values of 0.25 microseconds, 0.5 microseconds, and 1 microsecond, respectively. These combinations of the peak reverse recovery current and period t_B produce a reverse [dJ/dt] ranging from 5.7 to 7 x 10^9 A/cm^2-s.

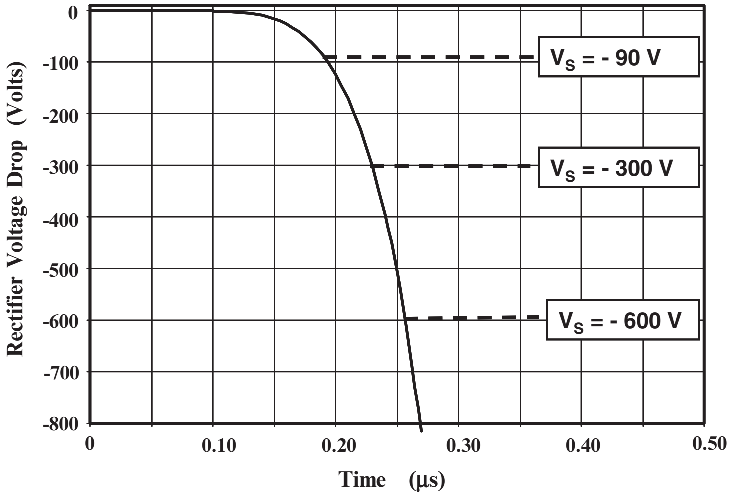

Fig. 6.15 Analytically Calculated Voltage Waveforms for a 1000 V P-i-N Rectifier during the Reverse Recovery Process for various Supply Voltages.

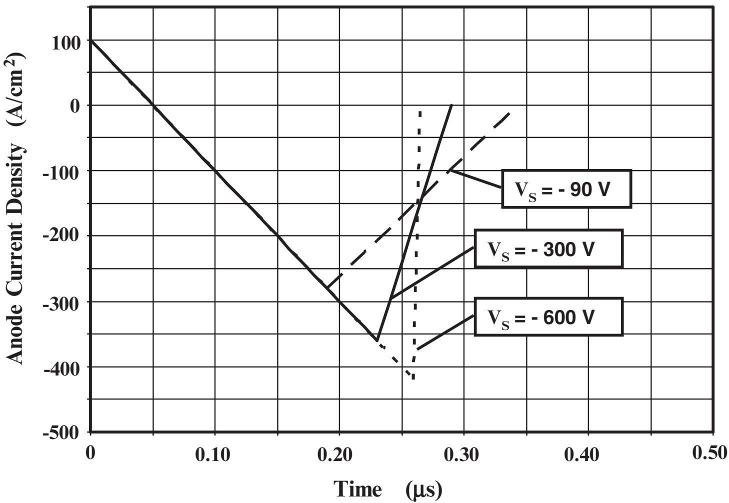

Fig. 6.16 Analytically Calculated Current Waveforms for a 1000 V P-i-N Rectifier during the Reverse Recovery Process for various Supply Voltages.

The analytical model also enables analysis of the impact of changing the reverse recovery voltage on the reverse recovery process. Consider the case of the same 1000 V P-i-N rectifier structure switched off from an on-state current density of 100 A/cm^2 at a ramp rate of 2 x 10^9 A/cm^2-s. The voltage waveform predicted by the analytical model is shown in Fig. 6.15 with dashed lines indicating the point at which the reverse bias voltage reaches values of 90, 300, and 600 volts during the reverse recovery transient. As the reverse voltage is increased, it takes a longer time interval to produce the wider space-charge region that is needed to support the voltage. This is accompanied by a larger value for the peak reverse recovery current as shown in Fig. 6.16. The larger space-charge region, formed at larger reverse bias voltages, removes a greater fraction of the stored charge as well. This produces a substantial reduction of the period t_B resulting in very high reverse [dJ/dt] as observed in the figure.

The peak reverse recovery current density predicted by the analytical model increases from 280 to 360 to 420 A/cm^2, when the voltage is increased from 90 to 300 to 600 volts, respectively, as can be observed from Fig. 6.16. The time duration (t_B) for the fourth phase, during which the reverse current reduces to zero, also becomes smaller with an increase in the reverse voltage. The values for t_B predicted by the analytical model are 153 nanoseconds, 60 nanoseconds, and only 1 nanosecond for reverse voltages of 90, 300, and 600 volts, respectively. The t_B value for the 600 volt case indicates that almost all the stored charge has been extracted by the extension of the space-charge region at this large reverse voltage. These combinations of the peak reverse recovery current and period t_B produce a drastic increase in the reverse [dJ/dt] ranging from 1.8 to 6 to 420 x 10^9 A/cm^2-s when the reverse voltage is increased from 90 to 300 to 600 volts, respectively.

Simulation Example

In order to validate the above model for the reverse recovery transient in the P-i-N rectifier, the results of numerical simulations on a 1000 V silicon P-i-N rectifier structure are described here. The structure had a drift region thickness of 60 microns with a doping concentration of 5 x 10^{13} cm^{-3}. The cathode current was ramped from 100 A/cm^2 in the on-state using various values of negative ramp rates. In addition, the impact of changing the lifetime and the reverse supply voltage was examined for comparison with the analytical model.

First consider the case of varying the negative ramp rate from 1 x 10^9 to 2 x 10^9 to 4 x 10^9 A/cm^{2}s. For these cases, a lifetime (τ_{p0} and τ_{n0}) value of 1 microsecond was used during the numerical simulations. The average carrier concentration in the drift region under steady state conditions with an on-state current density of 100 A/cm^2 was found to be about 5 x 10^{16} cm^{-3} as shown in Fig. 6.8E. This value is obtained by using a high level lifetime of 0.5 microseconds in Eq. [6.59] indicating that end-region recombination currents are significant in this structure. The carrier concentration profile exhibits a zero slope at time t = 40 ns, corresponding to time $t = t_0$ in the analytical model (see Fig. 6.8]. The slope of the carrier profile then becomes positive, as shown for the time t = 80 ns. During this time, the carrier concentration at the junction is well above the equilibrium value

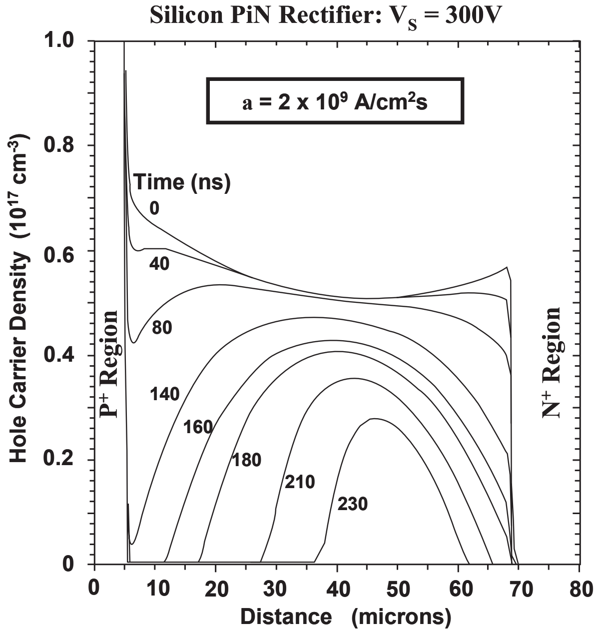

Fig. 6.8E Carrier Distribution in a 1000V Silicon P-i-N Rectifier during Phase 1, 2 and 3 of the Reverse Recovery Transient.

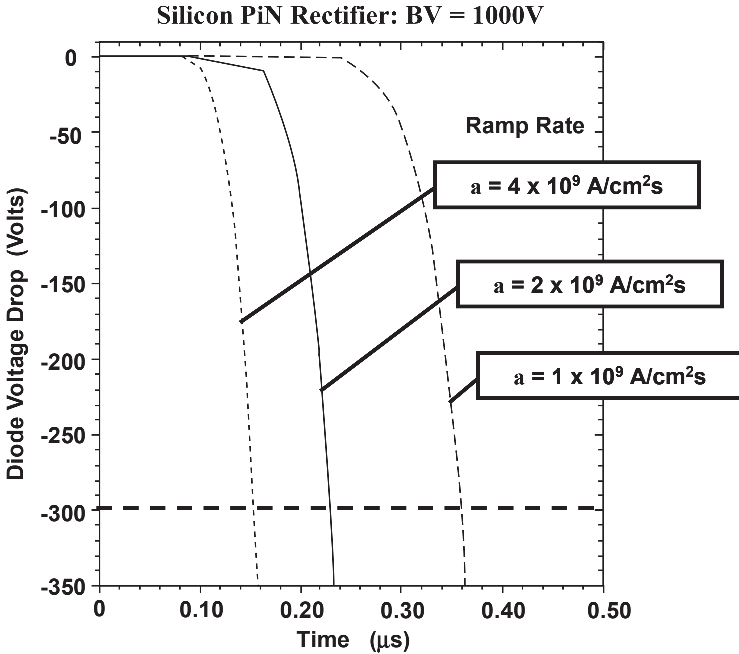

Fig. 6.9E Voltage Waveforms for a 1000V Silicon P-i-N Rectifier during the Reverse Recovery Transient with various Ramp Rates.

indicating that the P^+/N junction is still forward biased. At time t = 140 ns, the carrier concentration at the junction becomes close to zero, corresponding to the time $t = t_1$ in the analytical model (see Fig. 6.8). The value for t_1 obtained using the analytical model is about 120 ns in good agreement with the simulations.

The carrier profiles for subsequent time instances of 160, 180, 210, and 230 ns are also shown in Fig. 6.8E. It can be observed that the depletion region expands from the P^+/N junction during this time interval. The analytical model predicts a depletion region width of 38 microns, when the reverse bias voltage reaches 300 volts, in excellent agreement with the simulations. The analytical model also predicts the end of phase 3 at time t_2 = 230 ns in very good agreement with the simulations. Consequently, the peak reverse recovery current predicted by the model also agrees with the simulations

The diode voltage and current waveforms obtained with the aid of the numerical simulations are shown in Fig. 6.9E and 6.10E, respectively. These waveforms have the same features predicted by the analytical model (see Fig. 6.11 and Fig. 6.12). The peak reverse currents obtained using the model are in good agreement with those observed in the simulations. However, the transient observed with the numerical simulations during phase 4 occurs with a constant ramp rate followed by a more abrupt reduction of the current. The ramp rate observed with the simulations is in the range between 7 and 9 x 10^9 A/cm^2s as predicted by the analytical model.

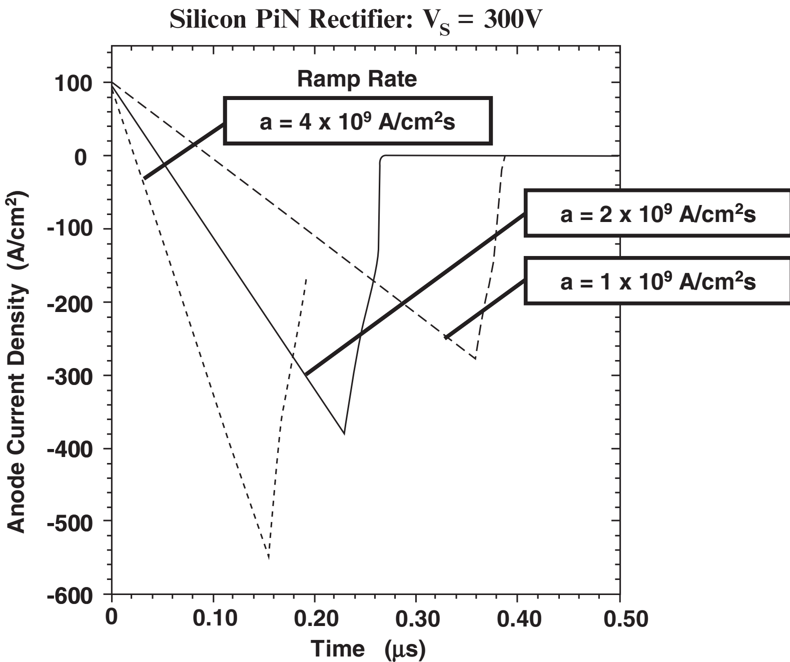

Fig. 6.10E Current Waveforms for a 1000V Silicon P-i-N Rectifier during the Reverse Recovery Transient with various Ramp Rates.

During the fourth phase of the turn-off process, the remaining free carriers in the drift region are removed by further extension of the depletion region as the current ramps down to zero. The reduction of the reverse current is accompanied by a reduction in the concentration of holes within the space-charge region as described by Eq. [6.80]. This reduces the net positive charge in the space-charge region allowing its expansion in spite of the constant reverse voltage across the diode. Since the P-i-N rectifier is designed with a punch-through architecture, the space-charge region eventually expands through the entire drift region removing all the stored charge. The removal of the stored charge, observed with the numerical simulations, is shown in Fig. 6.11E.

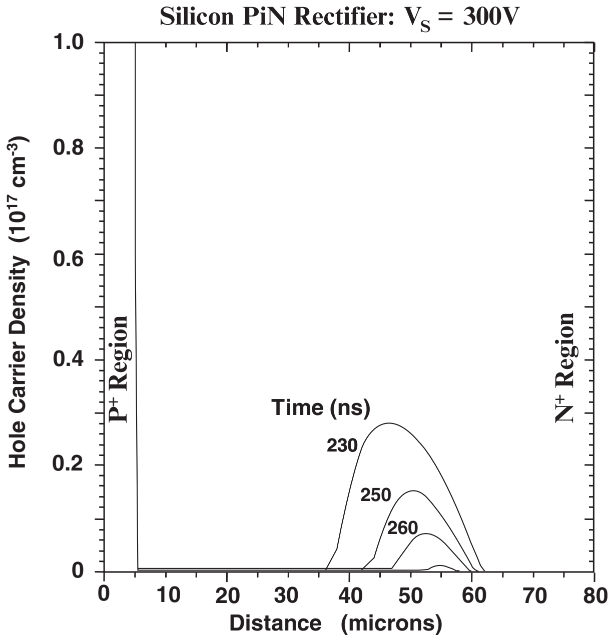

Fig. 6.11E Carrier Distribution in a 1000V Silicon P-i-N Rectifier during Phase 4 of the Reverse Recovery Transient.

The validity of the analytical model can also be examined by observation of the impact of changes in the lifetime on the reverse recovery process. In order to illustrate this, the lifetime was increased and reduced by a factor of 2x while performing the reverse recovery at ramp rate of 2 x 10^9 A/cm^{2}s. The diode voltage and current waveforms obtained using the numerical simulations are shown in Fig. 6.12E and 6.13E, respectively.

The waveforms shown in the above figures have the same features as the waveforms obtained using the analytical model (see Fig. 6.13 and 6.14). There is no change in the time t_1 for the end of the second phase while the time taken for the voltage to increase to 300 volts reduces with a reduction in the lifetime. The peak reverse recovery current decreases with a reduction of the lifetime as predicted by the model. The time duration for the fourth phase also increases with increasing lifetime as predicted by the model, resulting in a slightly smaller reverse [di/dt].

It can be concluded that the analytical model provides an accurate description of the impact of changes in the lifetime on the reverse recovery process.

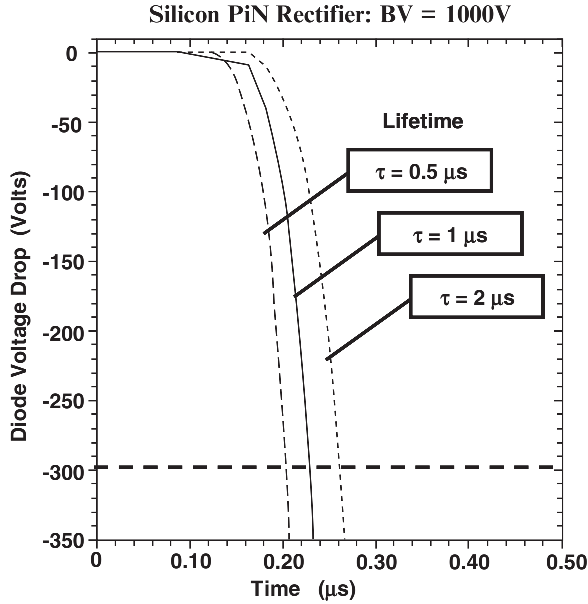

Fig. 6.12E Voltage Waveforms for a 1000V Silicon P-i-N Rectifier during the Reverse Recovery Transient with various Lifetimes.

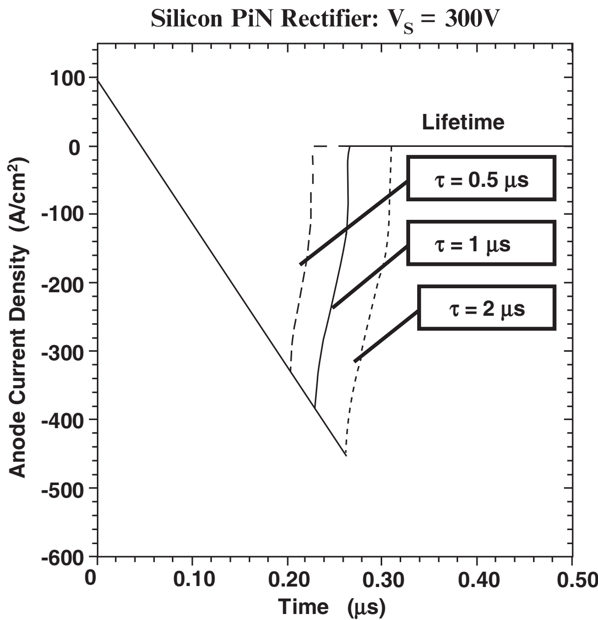

Fig. 6.13E Current Waveforms for a 1000V Silicon P-i-N Rectifier during the Reverse Recovery Transient with various Lifetimes.

As a further validation of the model, numerical simulations of the 1000 V P-i-N rectifier structure were performed with various reverse bias supply voltages. The voltage waveform is shown in Fig. 6.14E for the case of a ramp rate of 2 x 10^9 A/cm^{2}s and lifetime of 1 microsecond. The time taken to arrive at the increasing reverse bias voltages is consistent with the prediction of the analytical model (see Fig. 6.15). Consequently, the peak reverse recovery currents predicted by the analytical model are also in agreement with those obtained from the numerical simulations. These waveforms are shown in Fig. 6.15E.

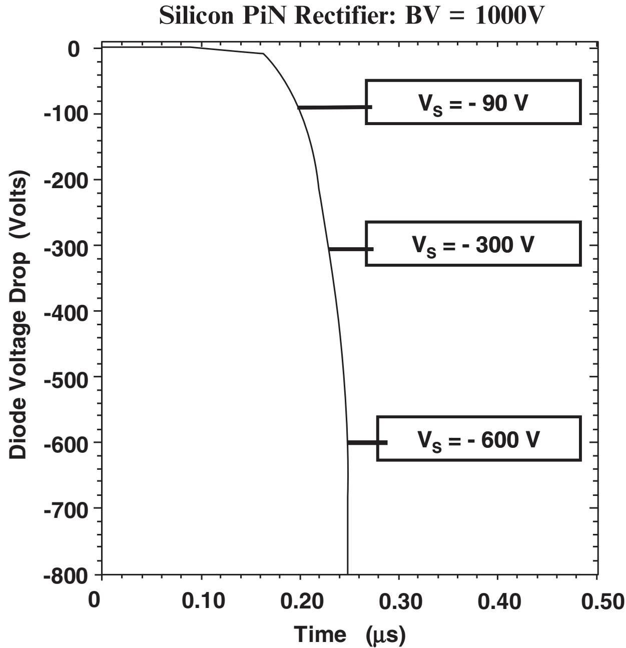

Fig. 6.14E Voltage Waveforms for a 1000V Silicon P-i-N Rectifier during the Reverse Recovery Transient with various Supply Voltages.

The current waveforms observed with the numerical simulations have the same features predicted by the analytical model (see Fig. 6.16). When the reverse voltage is increased to 600 volts, the fourth phase of the reverse recovery occurs with an abrupt reduction of the reverse current as predicted by the analytical model. The peak reverse currents obtained using the model are also in good agreement with those observed in the simulations. The extremely high reverse [di/dt] associated with an abrupt drop in the reverse recovery current is a problem in power circuits where it produces large voltage spikes across any stray inductances that are in series with the diode.

The above simulation results provide validation for the analytical model developed in this section of the chapter and give additional insight into the carrier distribution and transients. Based upon the excellent match between the predictions of the analytical model and the simulations, it can be concluded that the model is

able to account for the all four phases of the reverse recovery process and predict the proper dependence of the reverse recovery current on the ramp rate, the lifetime, and the reverse supply voltage.

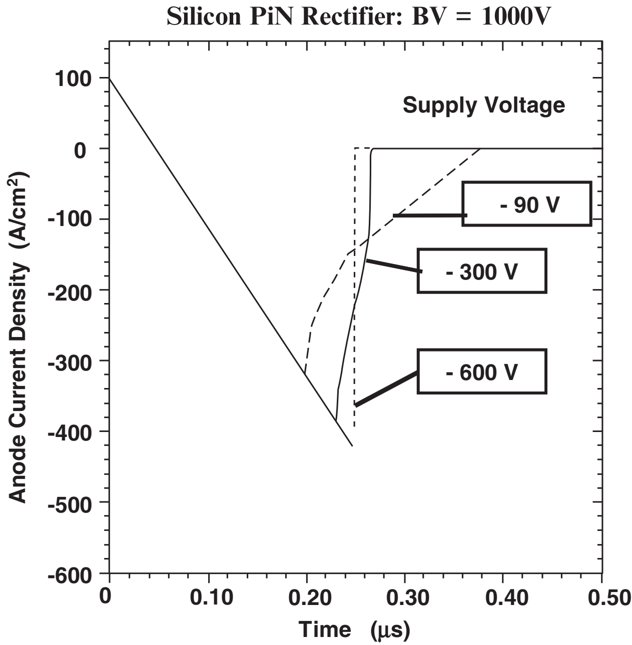

Fig. 6.15E Current Waveforms for a 1000V Silicon P-i-N Rectifier during the Reverse Recovery Transient with various Supply Voltages.

6.5 P-i-N Rectifier Trade-Off Curves

In the previous sections, it was demonstrated that the peak reverse recovery current and the turn-off time can be reduced by reducing the minority carrier lifetime in the drift region of the P-i-N rectifier structure. This enables reduction of the power losses during the switching transient. However, the on-state voltage drop in a P-i-N rectifier increases when the minority carrier lifetime is reduced, which produces an increase in the power dissipation during on-state current flow. For power system applications, it is desirable to reduce the total power dissipation produced in the rectifiers to maximize the power conversion efficiency. This also reduces the heat generated within the power devices maintaining a lower junction temperature which is desirable to prevent thermal runaway and reliability problems. To minimize the power dissipation, it is common-place to perform a trade-off between on-state and switching power losses for power P-i-N rectifiers by developing trade-off curves.

One type of the trade-off curve for a power P-i-N rectifier can be generated by plotting the on-state voltage drop against the reverse recovery turn-off time.

A turn-off waveform that includes a non-linear portion during the fourth phase is illustrated in Fig. 6.17. The turn-off time (t_{rr}) is defined as the time taken for the reverse current to reduce to 10 percent of the peak reverse recovery current (J_{PR}) after the current crosses zero. This time can be extracted from the measured characteristics of devices using automated test equipment. In addition, it is common practice to extract the times t_A and t_B as defined on the waveform in Fig. 6.17. A larger [t_B/t_A] ratio is considered to be desirable to mitigate the voltage spikes created in power circuits by a large [di/dt] in the reverse direction.

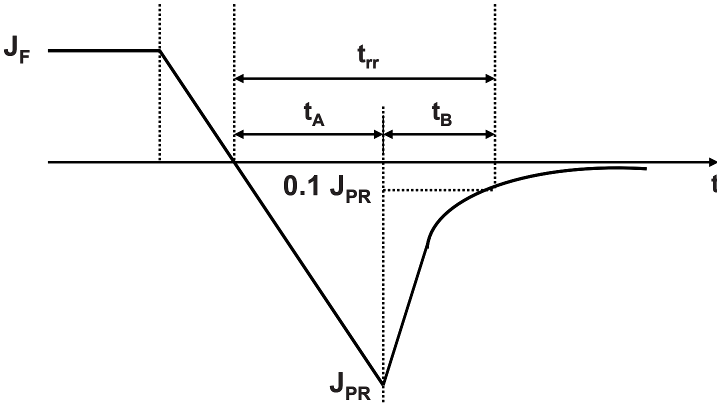

Fig. 6.17 Typical Reverse Recovery Current Waveform for the P-i-N rectifier Structure defining the Reverse Recovery Turn-Off Time.

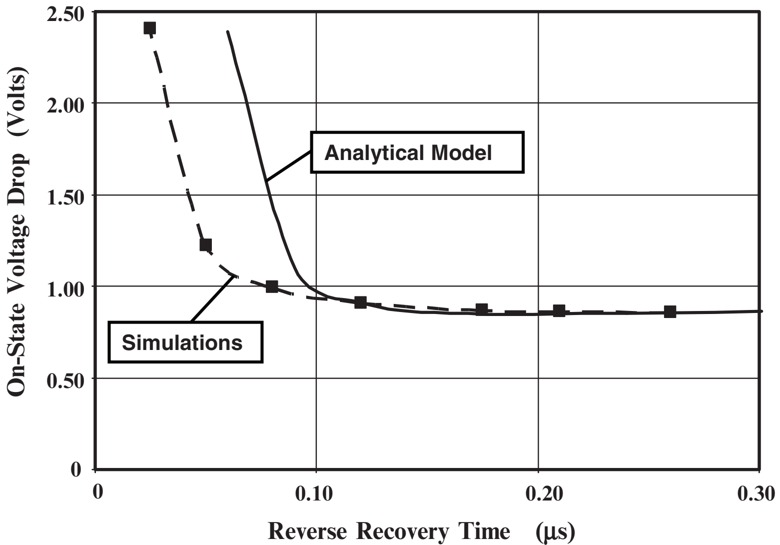

Fig. 6.18 Trade-Off Curve for the Punch-Through P-i-N rectifier Structure.

The trade-off curve between the on-state voltage drop and the reverse recovery time obtained by using the analytical models is shown in Fig. 6.18 by the solid line. The results obtained using two dimensional numerical simulations for the punch-through structure are also shown in the figure for comparison. It can be observed that there is good agreement between them until the lifetime is reduced below 0.05 microseconds to achieve a reverse recovery time of less than 0.1 microseconds. The reverse recovery time predicted by the analytical models is larger than observed with the simulations because free carrier recombination was neglected during the reverse recovery process. This assumption is not valid when the recombination lifetime is reduced to below 0.05 microseconds.

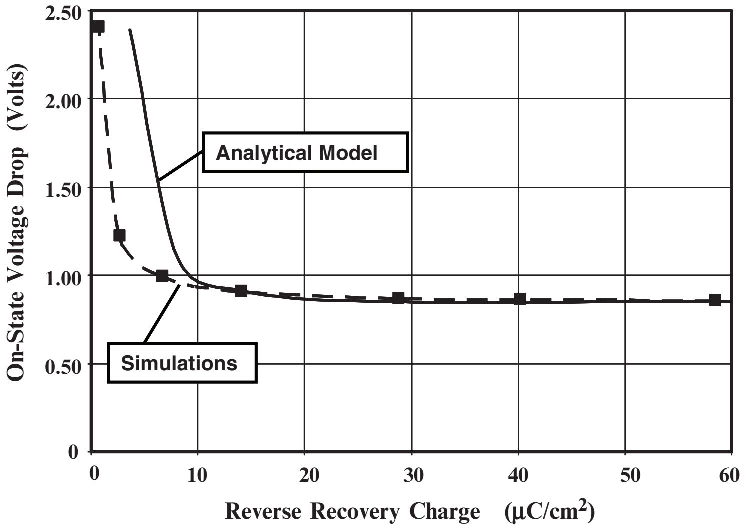

Fig. 6.19 Trade-Off Curve for the Punch-Through P-i-N rectifier Structure.

Another common practice for displaying the trade-off in power losses in power P-i-N rectifiers is by plotting the on-state voltage drop against the reverse recovery charge (Q_{rr}). The reverse recovery charge can be extracted by integration of the turn-off waveform for the current. This graph obtained with the analytical model and the simulations is shown in Fig. 6.19 for the punch-through structure.

6.6 Summary

The physics of operation of the P-i-N rectifier has been analyzed in this chapter. Analytical expressions have been derived for the on-state and blocking state, as well as the reverse recovery transients. At on-state current levels, the injected minority carrier density in the drift region exceeds the relatively low doping concentration required to achieve high breakdown voltages. This high level injection in the drift region modulates its conductivity producing a reduction in the

on-state voltage drop. If recombination in the drift region is dominant, the voltage drop across the drift region becomes independent of the on-state current density. These phenomena allow operation of the silicon P-i-N rectifier with an on-state voltage drop of only 1 volt making it very attractive for power electronic applications.

The P-i-N rectifier can support a large voltage in the reverse blocking mode by appropriate choice of the doping concentration and thickness of the drift region. A punch-through design is favored because it reduces the thickness of the drift region. A narrower drift region contains a smaller amount of stored charge during on-state operation enabling faster turn-off.

The switching of the P-i-N rectifier from the on-state to the reverse blocking state is accompanied by a significant current flow in the reverse direction. This reverse current produces large power dissipation in the rectifier as well as the power switches in power converter circuits. The reverse recovery current and the reverse recovery turn-off time can be reduced by reduction of the recombination lifetime in the drift region. Since this is accompanied by an increase in the on-state voltage drop, it is customary to perform a trade-off analysis to minimize the overall power dissipation.

Silicon carbide based P-i-N rectifiers have a much narrower drift region thickness when compared with silicon devices due to the higher critical electric field for breakdown. This favors a faster switching speed with reduced reverse recovery current. However, the larger band-gap for silicon carbide produces an on-state voltage drop that is four times larger than for the silicon rectifiers. For this reason, silicon carbide P-i-N rectifiers are of interest only when the blocking voltage capability exceeds 10,000 volts.

References

[1] B.J. Baliga, "Fundamentals of Power Semiconductor Devices", Springer Scientific, New York, 2008.

[2] B.J. Baliga, "Silicon Carbide Power Devices", World Scientific Publishing Company, 2005.

[3] S.K. Ghandhi, "Semiconductor Power Devices", pp. 112-128, John Wiley and Sons, 1977.

[4] R.N. Hall, "Power Rectifiers and Transistors", Proceedings of the IRE, Vol. 40, pp. 1512-1518, 1952.

[5] H. Benda and E. Spenke, "Reverse Recovery Processes in Silicon Power Rectifiers", Proceedings of the IEEE, Vol. 55, pp. 1331-1354, 1967.

[6] N.R. Howard and G.W. Johnson, "PIN Silicon Diodes at High Forward Current Densities", Solid State Electronics, Vol. 8, pp. 275-284, 1965.

[7] A. Herlet, “The Forward Characteristics of Silicon Power Rectifiers at High Current Densities”, Solid State Electronics, Vol. 11, pp. 717-742, 1968.
[8] Q. Zhang, et al, “12-kV p-Channel IGBTs with Low On-Resistance in 4H-SiC”, IEEE Electron Device Letters, Vol. EDL-29, pp. 1027-1029, 2008.